Dynamic localization of the chromosomal passenger complex is controlled by the orphan kinesin KIN-A in the kinetoplastid parasite *Trypanosoma brucei*

Daniel Ballmer[1] and Bungo Akiyoshi[1,2,*]

[1]Department of Biochemistry, University of Oxford, South Parks Road, Oxford, OX1 3QU, United Kingdom

[2]The Wellcome Centre for Cell Biology, Institute of Cell Biology, School of Biological Sciences, Edinburgh, EH9 3BF, United Kingdom

[*]Correspondence to bungo.akiyoshi@ed.ac.uk

Abstract

The chromosomal passenger complex (CPC) is an important regulator of cell division, which shows dynamic subcellular localization throughout mitosis, including kinetochores and the spindle midzone. In traditional model eukaryotes such as yeasts and humans, the CPC consists of the catalytic subunit Aurora B kinase, its activator INCENP, and the localization module proteins Borealin and Survivin. Intriguingly, Aurora B and INCENP as well as their localization pattern are conserved in kinetoplastids, an evolutionarily divergent group of eukaryotes that possess a unique set of kinetochore proteins and lack homologs of Borealin or Survivin. It is not understood how the kinetoplastid CPC assembles or how it is targeted to its subcellular destinations during the cell cycle. Here, we identify two orphan kinesins, KIN-A and KIN-B, as bona fide CPC proteins in *Trypanosoma brucei*, the causative agent of African sleeping sickness. By employing biochemical, structural, and cell biological approaches, we demonstrate that KIN-A and KIN-B serve as the scaffold for the assembly of the remaining CPC subunits. Kinetochore localization of the CPC depends on the KKT7 – KKT8 complex pathway, with the C-terminal unstructured tail of KIN-A serving as a key interaction partner for the KKT8 complex. Our data therefore show that, unlike other eukaryotes that take advantage of histone modifications for centromere recruitment, trypanosomes rely on kinetochore proteins to recruit the CPC onto kinetochores. Furthermore, the kinesin motor activity of KIN-A promotes chromosome alignment in prometaphase and CPC translocation to the central spindle upon anaphase onset. Thus, KIN-A constitutes a unique 'two-in-one' CPC localization module, directing the CPC to kinetochores (from S phase until metaphase) via its C-terminal tail, and to the central spindle (in anaphase) via its N-terminal kinesin motor domain. Our findings highlight the evolutionary diversity of CPC proteins and raise the possibility that kinesins may have served as the original transport vehicles for Aurora B kinases in early eukaryotes.

Introduction

During cell division, duplicated genetic material must be distributed equally into two daughter cells. The Aurora B kinase is a key mitotic regulator widely conserved among eukaryotes (Hochegger et al., 2012). It undergoes dynamic localization changes throughout mitosis to enable the spatially restricted phosphorylation of substrates involved in chromosome alignment, chromosome bi-orientation, spindle assembly checkpoint (SAC) signalling and cytokinesis (Carmena et al., 2012). In early mitosis, Aurora B is first detected on chromosome arms and during prometaphase becomes enriched at centromeres, where it destabilizes incorrect kinetochore-microtubule attachments (Krenn and Musacchio, 2015). Upon anaphase onset, Aurora B translocates to the spindle midzone, and during cytokinesis associates with the equatorial cortex to regulate cell abscission (Adams et al., 2000; Cooke et al., 1987; Trivedi and Stukenberg, 2016).

The dynamic localization pattern of the Aurora B kinase is in part achieved through its association with a scaffold comprised of inner centromere protein (INCENP), Borealin and Survivin (Adams et al., 2001, 2000; Gassmann et al., 2004; Romano et al., 2003; Sampath et al., 2004; Vader et al., 2006; Wheatley et al., 2001). Together, these proteins form a tetrameric complex referred to as the chromosomal passenger complex (CPC). The CPC can be partitioned into two functional modules: The 'catalytic module' and the 'localization module'. The catalytic module is composed of Aurora B in complex with the IN-box at the INCENP C-terminus, which is required for full activation of the Aurora B kinase (Bishop and Schumacher, 2002). The localization module comprises Borealin and Survivin, which form a three-helical bundle with the N-terminal region of INCENP (Jeyaprakash et al., 2007, 2011; Klein et al., 2006). In vertebrates, recruitment of the CPC to centromeric chromatin depends on two pathways, involving the Haspin and Bub1 kinases. Haspin phosphorylates histone H3 on Thr3 (H3T3ph), which is recognized by the baculovirus IAP repeat (BIR) domain of Survivin (Kelly et al., 2010; Wang et al., 2010; Yamagishi et al., 2010). H3T3ph is initially found along the entire length of chromosomes between sister chromatids but becomes enriched at the inner centromere (the space between sister kinetochores) during late prophase. In contrast, the kinetochore-associated Bub1 kinase phosphorylates histone H2A on Thr120 (H3AT120ph) (Kawashima et al., 2010). H2AT120ph recruits Shugoshin-like proteins (Sgo1 and Sgo2), which in turn are bound by Borealin (Tsukahara et al., 2010; Yamagishi et al., 2010). Recently, Sgo1 has also been demonstrated to interact with the BIR domain of Survivin through an N-terminal histone H3-like motif (Abad et al., 2022; Jeyaprakash et al., 2011). The interactions of Borealin and Survivin with Sgo1 form the basis for a kinetochore-proximal pool of the CPC which is distinct from the inner centromere pool (Broad et al., 2020; Hadders et al., 2020; Liang et al., 2020).

68 In most studied eukaryotes, ranging from yeast to humans, kinetochore assembly is scaffolded
69 by a centromere-specific histone H3 variant, CENP-A (Allshire and Karpen, 2008; Black and Cleveland,
70 2011; Hori and Fukagawa, 2012; Maddox et al., 2012; Westhorpe and Straight, 2013). An assembly of
71 inner kinetochore protein complexes, referred to as the constitutive centromere-associated network
72 (CCAN), interacts with centromeric CENP-A chromatin throughout the cell cycle and provides a
73 platform for recruitment of the outer kinetochore KNL1/Mis12 complex/Ndc80 complex (KMN)
74 network that has microtubule-binding activity (Cheeseman et al., 2006; Foltz et al., 2006; Izuta et al.,
75 2006; Okada et al., 2006). Some of these kinetochore proteins are present in nearly all sequenced
76 eukaryotes, suggesting that key principles of chromosome segregation are widely shared among
77 eukaryotes (Drinnenberg and Akiyoshi, 2017; Je Van Hooff et al., 2017; Meraldi et al., 2006; Tromer et
78 al., 2019). However, a unique set of kinetochore proteins (KKT1–20, KKT22–25, KKIP1–12) are present
79 in the evolutionarily divergent lineage called kinetoplastids (Akiyoshi, 2020; Akiyoshi and Gull, 2014;
80 D'Archivio and Wickstead, 2017; Nerusheva et al., 2019; Nerusheva and Akiyoshi, 2016).
81 Kinetoplastids are flagellated protists that are highly divergent from commonly studied eukaryotes
82 (Cavalier-Smith, 2010). *Trypanosoma brucei*, *Trypanosoma cruzi* and *Leishmania* spp. are causative
83 agents of African trypanosomiasis, Chagas disease and leishmaniasis, respectively, and as such pose a
84 serious threat to public health and prosperity across the tropics and subtropics (Stuart et al., 2008;
85 WHO, 2017).
86 Despite the absence of canonical kinetochore components (Berriman et al., 2005; Lowell and
87 Cross, 2004), Aurora kinases are conserved in kinetoplastids. Early studies suggested that the Aurora
88 B homolog (Aurora B^{AUK1}) in *T. brucei* forms a complex with chromosomal passenger complex proteins
89 1 and 2 (CPC1 and CPC2) and plays a crucial role in mitosis and cytokinesis (Li et al., 2008; Tu et al.,
90 2006). CPC1 was later found to be a divergent INCENP homolog (hereafter referred to as $INCENP^{CPC1}$)
91 based on the presence of a conserved C-terminal IN-box (Hu et al., 2014). However, $INCENP^{CPC1}$ lacks
92 the central SAH domain and N-terminal residues, which in other eukaryotes interact with Survivin and
93 Borealin. Although homologs of the 'localization module' proteins Survivin and Borealin have not been
94 identified in kinetoplastids (Komaki et al., 2022), the trypanosome CPC displays a dynamic localization
95 pattern similar to that of the metazoan CPC (Li et al., 2008): Aurora B^{AUK1}, $INCENP^{CPC1}$ and CPC2 localize
96 to kinetochores in early mitosis and then translocate to the central spindle upon anaphase onset. From
97 late anaphase onwards, an additional population of CPC proteins is detectable at the tip of the new
98 flagellum attachment zone (FAZ), the point of cytokinesis initiation in *T. brucei*. It is presently not
99 understood how the CPC assembles in these evolutionarily divergent eukaryotes nor how its
100 localization dynamics are regulated during the cell cycle.

101 Here, by combining biochemical, structural and cell biological approaches, we show that the
102 trypanosome CPC is a pentameric complex comprising Aurora B^{AUK1}, $INCENP^{CPC1}$, CPC2 and the two
103 orphan kinesins KIN-A and KIN-B. KIN-A and KIN-B interact via their coiled-coil domains to form a
104 subcomplex within the CPC, which serves as a scaffold for assembly of the catalytic module (Aurora
105 B^{AUK1} + $INCENP^{CPC1}$). The C-terminal unstructured tail of KIN-A directs kinetochore localization of the
106 CPC from S phase to metaphase, while the N-terminal motor promotes the central spindle enrichment
107 in anaphase. Furthermore, we identify the KKT7 – KKT8 complex pathway as the main kinetochore
108 recruitment arm of the trypanosome CPC.

109

110 ## Results

111

112 **KIN-A and KIN-B are bona fide CPC proteins in trypanosomes**

113 To identify additional interactors of the CPC in trypanosomes, we performed immunoprecipitation
114 followed by liquid chromatography tandem mass spectrometry (IP-MS) of endogenously YFP-tagged
115 Aurora B^{AUK1} (Fig. 1A and Table S2). Besides $Aurora^{AUK1}$, $INCENP^{CPC1}$ and CPC2, we observed notable
116 enrichment of two orphan kinesins, KIN-A and KIN-B (Wickstead and Gull, 2006), as reported
117 previously (Li et al., 2008). Both KIN-A and KIN-B were also highly enriched in immunoprecipitates of
118 ectopically expressed GFP-NLS-$INCENP^{CPC1}$. Furthermore, IP-MS against GFP-NLS-KIN-A and GFP-NLS-
119 KIN-B identified Aurora B^{AUK1}, $INCENP^{CPC1}$ and CPC2 as top hits (Fig. S1A and Table S2).

120 We next assessed the localization dynamics of fluorescently tagged KIN-A and KIN-B over the
121 course of the cell cycle (Figs. 1, B-E). Unexpectedly, both KIN-A-YFP and GFP-KIN-B exhibited a CPC-
122 like localization pattern similar to that of Aurora B^{AUK1}: Both kinesins localized to kinetochores from S
123 phase to metaphase, and then translocated to the central spindle in anaphase (Figs. 1, C-E). Moreover,
124 similarly to Aurora B^{AUK1}, a population of KIN-A and KIN-B localized at the new FAZ tip from late
125 anaphase onwards (Figs. S1, B and C). These data show that KIN-A and KIN-B are bona fide CPC proteins
126 in trypanosomes, associating with $Aurora^{AUK1}$, $INCENP^{CPC1}$ and CPC2 throughout the cell cycle.

127 A bioinformatic search for homologs of CPC proteins within Euglenozoa revealed that both
128 KIN-A and KIN-B are present in trypanosomatids and bodonids, with KIN-A homologs detectable even
129 in prokinetoplastids (Fig. S1D) (Materials and Methods). CPC2, on the other hand, was detectable only
130 within trypanosomatids. Aurora B^{AUK1} and $INCENP^{CPC1}$ are present in kinetoplastids as well as in
131 diplonemids and euglenids (sister groups of kinetoplastids). Interestingly, homologs of Borealin,
132 Survivin, KIN-A, or KIN-B were not detectable in diplonemids or euglenids, raising a possibility that
133 these organisms may also possess 'non-canonical' CPC proteins. We conclude that the KIN-A and KIN-

134 B kinesins are highly conserved within kinetoplastids, constituting integral components of the CPC in
135 this evolutionary divergent group of eukaryotes.
136
137 **KIN-A promotes kinetochore localization of the CPC**
138 To investigate which subunits of the CPC are responsible for its kinetochore targeting, we performed
139 a series of RNAi experiments (Figs. 2, A-E). As previously reported (Li et al., 2008), depletion of Aurora
140 B^{AUK1}, $INCENP^{CPC1}$, KIN-A or KIN-B resulted in a prominent growth defect (Fig. S2A) with cells arresting
141 in G2/M (2K1N) (Fig. S2B). Depleting CPC2 using two different hairpin RNAi constructs (Materials and
142 Methods) had only a moderate impact on cell growth and cell cycle progression, and did not noticeably
143 affect the kinetochore localization of the other CPC subunits (Figs. S2, A-D). For this reason together
144 with to its limited conservation among kinetoplastids (Fig. S1D), we did not include CPC2 for further
145 analysis in this study. Knockdown of Aurora B^{AUK1} did not affect the kinetochore localization of YFP-
146 tagged $INCENP^{CPC1}$, KIN-A or KIN-B (Figs. 2, A and C-E). Knockdown of $INCENP^{CPC1}$ caused delocalization
147 of Aurora B^{AUK1} but not of KIN-A or KIN-B (Figs. 2, A and B, D and E). In contrast, both Aurora B^{AUK1} and
148 $INCENP^{CPC1}$ were delocalized upon depletion of KIN-A or KIN-B (Figs. 2, A-C). RNAi against KIN-A
149 affected KIN-B levels and vice versa (Figs. 2, A, D and E), indicating that KIN-A and KIN-B are not stable
150 in the absence of KIN-B or KIN-A, respectively.
151 We next ectopically expressed GFP-tagged truncations of KIN-A and KIN-B to assess which
152 domains promote their kinetochore targeting. Both KIN-A and KIN-B contain an N-terminal kinesin
153 motor domain followed by several predicted coiled-coil motifs (Li et al., 2008), although KIN-B is
154 predicted to be an inactive motor (Wickstead and Gull, 2006). In addition, KIN-A has a long C-terminal
155 tail. Unlike full-length KIN-B, KIN-B^{2-316} (inactive motor domain) failed to enrich at kinetochores and
156 was instead found in the nucleolus (Fig. S2, E and F). KIN-A^{2-309} (motor domain) was also primarily
157 detected in the nucleolus, although we observed additional spindle and weak kinetochore-like signal
158 in some metaphase cells (Fig. 2G). By contrast, both KIN-$A^{310-862}$ (coiled-coil domain + C-terminal
159 disordered tail) and KIN-$B^{317-624}$ (coiled-coil domain) clearly localized to kinetochores from S phase to
160 metaphase (Fig. 2H; Fig. S2G). Intriguingly, unlike endogenously YFP-tagged KIN-A, ectopically
161 expressed GFP-NLS fusions of both full-length KIN-A and KIN-$A^{310-862}$ were detectable at kinetochores
162 even in anaphase (Figs. 2, F and H), implying that KIN-A is primarily responsible for kinetochore
163 targeting of the CPC. GFP-NLS fusions of the central coiled-coil domain or the C-terminal disordered
164 tail of KIN-A did not localize to kinetochores (data not shown). These results show that kinetochore
165 localization of the CPC is mainly mediated through KIN-A and requires both the central coiled-coil
166 domain as well as the C-terminal disordered tail.
167

168 **Structural model of the trypanosome CPC**

169 To gain structural insights into the trypanosome CPC, we performed bis(sulfosuccinimidyl) suberate
170 (BS^3) cross-linking of native CPC complexes isolated by immunoprecipitation of endogenously tagged
171 YFP-Aurora B^{AUK1} from cells arrested prior to anaphase, followed by mass spectrometry analysis (IP-
172 CLMS) (Fig. 3A and Table S2). Our IP-CLMS data revealed high-score crosslinks between the predicted
173 coiled-coil domains of KIN-A and KIN-B, suggesting that the two kinesins form a parallel heterodimer.
174 As expected, Aurora B^{AUK1} formed contacts with the C-terminal IN-box of $INCENP^{CPC1}$, consistent with
175 these two proteins constituting the catalytic module of the CPC. The N-terminal region of $INCENP^{CPC1}$
176 interacted mainly with KIN-B and to a lesser degree with KIN-A, with most contacts confined to the N-
177 terminal ends of the predicted coiled-coil domains of the kinesins close to their motor domains. The
178 N-terminus of CPC2, on the other hand, formed crosslinks with the coiled-coil domain of KIN-A. In
179 summary, our crosslinking data on native CPCs suggest that Aurora B^{AUK1} forms a subcomplex with the
180 C-terminus of $INCENP^{CPC1}$, and that $INCENP^{CPC1}$ and CPC2 interact with the coiled-coil domain of KIN-
181 A:KIN-B via their N-terminal domains.

182 We next used AlphaFold2 (AF2) (Jumper et al., 2021; Mirdita et al., 2022) to predict the overall
183 structure of the trypanosome CPC by testing combinations of full-length Aurora B^{AUK1}, $INCENP^{CPC1}$,
184 CPC2, KIN-A and KIN-B, and truncations thereof (Figs. S3, A-D). In line with our IP-CLMS data, AF2
185 confidently predicted parallel coiled coils between KIN-A and KIN-B, with the main region of
186 interaction contained within the central region of KIN-A (residues ~310–550) and the C-terminal
187 region of KIN-B (residues ~320–580). The C-terminal tail (residues ~550–862) of KIN-A is predicted to
188 be intrinsically disordered (pLDDT scores <20, Fig. S3, A and B). Consistent with our crosslinking data,
189 the first ~55 residues of $INCENP^{CPC1}$, predicted to form two α-helices (residues ~7–21 and ~37–55),
190 interact with the coiled coils of KIN-A:KIN-B in close proximity to the kinesin motors. A flexible central
191 linker in $INCENP^{CPC1}$ bridges the N-terminus of $INCENP^{CPC1}$ and the catalytic module of the CPC (Aurora
192 B^{AUK1} + $INCENP^{CPC1}$ IN-box). Similarly to $INCENP^{CPC1}$, an N-terminal α-helical region in CPC2 (residues
193 ~19–75) interacts with the KIN-A:KIN-B coiled coils immediately downstream of the $INCENP^{CPC1}$ binding
194 site. Consistent with these predictions, $INCENP^{CPC1\ 2\text{-}147}$ and $CPC2^{2\text{-}120}$ displayed normal localization
195 dynamics indistinguishable from the corresponding full-length constructs (Figs. S3, E-F and H-I). In
196 contrast, GFP-NLS fusions of $INCENP^{CPC1}$ and CPC2 lacking their N-terminal domains failed to localize
197 to kinetochores (Figs. S3, G and J).

198 We then used PyXLinkViewer (Schiffrin et al., 2020) to map our IP-CLMS data onto the
199 assembled AF2 model of the trypanosome CPC (Fig. 3B). Using a Euclidian distance cut-off of 30 Å,
200 ~80% of crosslinks were compatible with the model, providing confidence in the AF2 predictions. The
201 few crosslinks that violated the distance constraints mainly represent intra-protein contacts between

202 the INCENP^{CPC1} N- and C-terminal domains or inter-protein contacts between the INCENP^{CPC1} C-
203 terminal domain and the kinesin motor domain of KIN-A. The central domain of INCENP^{CPC1} is predicted
204 to be unstructured (pLDDT scores <20, Figs. S3, B-D) and may act as a flexible linker, permitting
205 multiple orientations of the catalytic module relative to the KIN-A:KIN-B scaffold. Taken together,
206 these data indicate that KIN-A and KIN-B interact via their coiled-coil domains, which serve as a
207 scaffold for the assembly of the remaining CPC subunits.
208
209 **The CPC is recruited to kinetochores through the KKT7 – KKT8 complex pathway**
210 Core components of the Haspin-H3T3ph and Bub1-H2AT120ph-Sgo1 pathways that control CPC
211 recruitment to the centromere in other model eukaryotes are not found in kinetoplastids (Berriman,
212 2005), and so far, no centromere-specific histone modifications and/or histone variants have been
213 uncovered in *T. brucei*. We reasoned that the centromere receptor(s) of the trypanosome CPC may lie
214 within the repertoire of unconventional kinetochore proteins present in kinetoplastids. Our IP-CLMS
215 approach failed to detect crosslinks between CPC subunits and other kinetochore components (Table
216 S2), possibly due to the transient nature of these interactions. Nevertheless, several KKT proteins were
217 commonly enriched in the immunoprecipitates of Aurora B^{AUK1}, CPC1, KIN-A and KIN-B, the most
218 abundant ones being KKT6, KKT7, KKT8, KKT9, KKT10, KKT11 and KKT12 (Fig. 1A; Fig. S1A and Table
219 S2). KKT7 is detected at kinetochores from S phase until the end of anaphase and recruits the KKT8
220 complex (comprising KKT8, KKT9, KKT11 and KKT12) (Akiyoshi and Gull, 2014; Ishii and Akiyoshi, 2020).
221 The KKT8 complex localizes at kinetochores from S phase and dissociates at the metaphase-anaphase
222 transition.
223 Using previously validated RNAi constructs (Akiyoshi and Gull, 2014; Llauró et al., 2018;
224 Marcianò et al., 2021), we found that knockdown of KKT7 or KKT9 resulted in dispersal of YFP-Aurora
225 B^{AUK1} from kinetochores in ~70% of cells (Figs. 4, A-D). In contrast, depletion of KKT1, KKT2, KKT3, KKT4,
226 KKT6, KKT10/19, KKT14 and KKT16 had little or no effect on YFP-Aurora B^{AUK1} localization (Figs. S4, A
227 and B). KIN-A-YFP was also lost from kinetochores upon RNAi-mediated depletion of KKT8 complex
228 subunits (Figs. S4, C and D). We next tested whether KKT7 or the KKT8 complex were able to recruit
229 Aurora B^{AUK1} to an ectopic locus using the LacI-LacO system (Landeira and Navarro, 2007). For these
230 experiments, we expressed GFP-NLS tagged KKT7$^{2-261}$ or KKT8 fused to the Lac repressor (LacI) in
231 trypanosomes containing an ectopic Lac operator (LacO) array stably integrated into rDNA repeats.
232 Consistent with the finding that KKT7 lies upstream of the KKT8 complex (Ishii and Akiyoshi, 2020),
233 GFP-NLS-KKT7$^{2-261}$-LacI recruited tdTomato-KKT8, -KKT9 and -KKT12 (Fig. S4E). Expression of both GFP-
234 NLS-KKT7$^{2-261}$-LacI and GFP-NLS-KKT8-LacI resulted in robust recruitment of tdTomato-Aurora B^{AUK1} to
235 LacO foci in S phase (Figs. 4, E and F). Intriguingly, we also noticed that, unlike endogenous KKT8 (which

236 is not present in anaphase), ectopically expressed GFP-NLS-KKT8-LacI remained at kinetochores during
237 anaphase (Fig. 4F). This resulted in a fraction of tdTomato-Aurora B^{AUK1} being trapped at kinetochores
238 during anaphase instead of migrating to the central spindle (Fig. 4F). We observed a comparable
239 situation upon ectopic expression of GFP-NLS-KIN-A, which is retained on anaphase kinetochores
240 together with tdTomato-KKT8 (Fig. S4F). In contrast, Aurora B^{AUK1} was not recruited to LacO foci
241 marked by GFP-NLS-$KKT7^{2-261}$-LacI in anaphase (Fig. 4E). These data suggest that the KKT8 complex
242 rather than KKT7 is the main kinetochore receptor of the CPC.
243
244 **KKT7 recruits the KKT8 complex via the KKT9:KKT11 subcomplex**
245 To gain further insight into the structure and assembly hierarchy within the KKT7 – KKT8 complex
246 pathway, we performed CLMS on native complexes isolated by immunoprecipitation of endogenously
247 YFP-tagged kinetochore proteins (Fig. 4G, Table S2) (Materials & Methods). We detected extensive
248 contacts between KKT8 and KKT12 as well as between KKT9 and KKT11, suggesting that KKT8:KKT12
249 and KKT9:KKT11 each form distinct subcomplexes. Additional crosslinks were detected between
250 KKT9:KKT11 and KKT8. To validate these findings, we co-expressed combinations of 6HIS-KKT8, KKT9,
251 KKT11 and KKT12 in *E. coli* and performed metal affinity chromatography (Fig. 4H). 6HIS-KKT8
252 efficiently pulled down KKT9, KKT11 and KKT12, as shown previously (Ishii and Akiyoshi, 2020). In the
253 absence of KKT9, 6HIS-KKT8 still pulled down KKT11 and KKT12. Removal of both KKT9 and KKT11 did
254 not impact formation of the KKT8:KKT12 subcomplex. In contrast, 6HIS-KKT8 was largely insoluble
255 without KKT12. Thus, KKT12 is required for formation of the full KKT8 complex. These results support
256 the idea that the KKT8 complex consists of KKT8:KKT12 and KKT9:KKT11 subcomplexes.
257 We next examined localization dependency of KKT8 complex components in cells. Using RNAi
258 constructs against individual subunits of the KKT8 complex (Akiyoshi and Gull, 2014; Ishii and Akiyoshi,
259 2020; Marcianò et al., 2021), we assessed localization of endogenously YFP-tagged KKT8, KKT9 and
260 KKT12 (Figs. S4, G-J). We found that knockdown of any subunit of the KKT8 complex affected protein
261 levels and kinetochore localization of the other subunits, indicating that presence of all subunits is
262 required to stabilize the full complex. YFP-KKT9 was least affected and was still detectable at
263 kinetochores in ~50% of cells depleted of KKT8, KKT11 or KKT12 (Fig. S4J). Thus, KKT9:KKT11 may lie
264 upstream of KKT8:KKT12. Indeed our IP-CLMS data suggest that the KKT9:KKT11 subcomplex directly
265 interacts with the N-terminus of KKT7 (Fig. 4G, Table S2). KKT7 also formed robust crosslinks with the
266 KKT10/19 kinases (Table S2), supporting our previous finding that KKT7 and KKT10 form a stable
267 complex (Ishii and Akiyoshi, 2020).

268 Consistent with our experimental data, AF2 predicted coiled coils between KKT8 and KKT12
269 and between KKT9 and KKT11 (Fig. 4I). The two subcomplexes are connected to each other through
270 interactions between the C-terminal end of the KKT8:KKT12 coiled coils and the C-terminus of KKT11.
271 Two alpha helices in KKT7$^{2-261}$ (residues ~149–181) are predicted to interact with KKT9:KKT11. Using a
272 distance cut-off of 30 Å, ~70% of crosslinks were compatible with the model. Of the crosslinks that
273 failed to meet the distance criteria, ~90% involved unstructured regions within KKT7 or the C-terminal
274 tail of KKT8. Collectively, our results reveal that KKT7 recruits the KKT8 complex through interaction
275 with the KKT9:KKT11 subcomplex (Fig. 4J). We propose that the KKT7 – KKT8 complex pathway serves
276 as the main CPC recruitment arm in trypanosomes.
277
278 **The KIN-A C-terminal tail interacts with the KKT8 complex through a conserved domain**
279 By IP-CLMS we failed to detect reliable crosslinks between the CPC and the KKT7 – KKT8 complex or,
280 in fact, any kinetochore proteins (Table S2). This suggests that the IP-CLMS approach, although well-
281 suited for characterizing stable protein complexes, may not be sensitive enough to detect transient or
282 lower affinity interactions. To overcome this, we used AF2 to probe for potential interactions between
283 the KKT8 and CPC (sub)complexes. AF2 did not predict interactions between the KKT8 complex and
284 INCENP^{CPC1}, CPC2 or KIN-B (data not shown). Intriguingly, AF2 predicted with high confidence
285 interactions between KKT9:KKT11 and a conserved region (residues ~722–741) within the KIN-A C-
286 terminal tail, which we termed conserved domain 1 (CD1) (Figs. 5, A and B). This interaction involves
287 a triple helix formed from KIN-A CD1, KKT9 and KKT11 in a region close to the KKT7 binding site. pLDDT
288 scores improved significantly for KIN-A CD1 in complex with KKT9:KKT11 (>80) compared to KIN-A CD1
289 alone (~20) (Figs. S3, A and B), suggesting that CD1 forms a helical structure upon binding to
290 KKT9:KKT11. CD1 can therefore be thought of as 'molecular recognition features' (Van Der Lee et al.,
291 2014), which undergo disorder-to-order transitions upon binding to their receptors.
292 Sequence alignment revealed the presence of a second conserved domain (residues ~816–
293 862) within the C-terminal tail of KIN-A, hereafter referred to as CD2 (Fig. 5B). To assess the
294 contributions of CD1 and CD2 for kinetochore recruitment of KIN-A in vivo, we ectopically expressed
295 GFP-NLS fusions of the central coiled coils and C-terminal tail of KIN-A (residues ~310–862) lacking
296 either CD1, CD2, or both (Figs. S5, A-D). GFP-NLS-KIN-A$^{310-862\ \Delta CD2}$ showed a moderate reduction in
297 kinetochore localization in metaphase and was completely lost from kinetochores in anaphase (Figs.
298 S5, B and E). By contrast, GFP-NLS-KIN-A$^{310-862\ \Delta CD1}$ was largely dispersed in metaphase but reappeared
299 at kinetochores in anaphase (Figs. S5, C and E). GFP-NLS-KIN-A$^{310-716}$ lacking both CD1 and CD2 failed
300 to localize at kinetochores both in metaphase and anaphase (Figs. S5, D and E). These data suggest

301 that CD1 and CD2 synergistically promote kinetochore localization of KIN-A, with CD1 interacting with
302 KKT9:KKT11 and CD2 likely interacting with another receptor at the kinetochore.
303 We next tested the relevance of KIN-A CD1 and CD2 for CPC localization and function by
304 replacing one allele of KIN-A with C-terminally tagged wild-type or mutant constructs lacking either
305 CD1 or CD2 and performed RNAi against the 3'UTR of KIN-A to deplete the untagged allele. We were
306 unable to obtain a rescue cell line lacking both CD1 and CD2 as the double-mutant protein was not
307 properly expressed. Wild-type KIN-A-YFP along with Aurora B^{AUK1} robustly localized to kinetochores
308 from S phase until anaphase onset (Figs. 1, C and D; Fig. 5C). KIN-$A^{\Delta CD1}$-YFP was detectable at
309 kinetochores in G2 but predominantly localized to the mitotic spindle from (pro)metaphase onwards
310 (Figs. 5, D and F), indicating that removal of CD1 severely weakens the affinity of KIN-A for
311 kinetochores and instead shifts the balance towards microtubule binding. Interestingly, expression of
312 KIN-$A^{\Delta CD1}$-YFP similarly affected the localization of Aurora B^{AUK1} (Figs. 5, D and G; Fig. S5F). We also
313 detected partial spindle localization of Aurora B^{AUK1} in a small population (~25%) of metaphase cells
314 expressing KIN-$A^{\Delta CD2}$-YFP (Figs. 5, E-G). Central spindle localization of KIN-A in anaphase was
315 unaffected by deletion of either CD1 or CD2 (Figs. 5, D and E). Remarkably, despite a substantial loss
316 of Aurora B^{AUK1} from kinetochores in metaphase, ΔCD1 cells exhibited normal cell cycle profiles (Fig.
317 S5G) and showed only a modest decrease in proliferation rates (Fig. 5H). This parallels the situation in
318 budding yeast, which can promote error-free chromosome segregation even when inner centromere
319 localization of Aurora B is largely abolished (Campbell and Desai, 2013; García-Rodríguez et al., 2019).
320
321 **CPC targeting to the central spindle in anaphase depends on KIN-A motor activity**
322 Finally, we asked how translocation of the CPC to the spindle midzone in anaphase is achieved in
323 trypanosomes. In mammalian cells, dephosphorylation of INCENP and the kinesin MKLP2 upon
324 anaphase onset allows formation of a transient CPC-MKLP2 complex (Gruneberg et al., 2004; Hümmer
325 and Mayer, 2009; Kitagawa et al., 2014; Serena et al., 2020). MKLP2 activity then drives plus-directed
326 movement of this complex along microtubules of the anaphase spindle. We therefore speculated that
327 anaphase translocation of the kinetoplastid CPC to the central spindle may be accomplished through
328 the kinesin motor domain of KIN-A. KIN-B is unlikely to be a functional kinesin based on the absence
329 of several well-conserved residues and motifs within the motor domain (Li et al., 2008). In line with
330 these possibilities, GFP-NLS fusions of the motor domain of KIN-A, but not KIN-B, localized to the
331 mitotic spindle (Fig. S2F). Microtubule co-sedimentation assays using recombinant proteins confirmed
332 that the kinesin motor domain of KIN-A but not KIN-B can bind microtubules in vitro (Fig. S6A).
333 Of note, ectopically expressed GFP-NLS-KIN-A and -KIN-A^{2-309} failed to concentrate at the
334 spindle midzone during anaphase (Figs. 2, F and G), suggesting that N-terminal tagging of the KIN-A

335 motor domain may perturb ATPase activity of the motor domain. To address whether the motor
336 activity of KIN-A is required for central spindle localization of the CPC, we replaced one allele of KIN-A
337 with a C-terminally YFP-tagged G209A ATPase-defective rigor mutant and used an RNAi construct
338 directed against the 3'UTR of KIN-A to deplete the untagged allele. We noticed that expression of the
339 rigor mutant slowed cell proliferation even in the presence of wild-type protein (Fig. 6G). The rigor
340 mutation did not affect recruitment of YFP-tagged KIN-A to kinetochores (Figs. S6, B and C). However,
341 KIN-A^{G209A}-YFP marked kinetochores were misaligned in ~50% of cells arrested in metaphase,
342 suggesting that motor activity of KIN-A promotes chromosome congression to the metaphase plate
343 (Figs. S6, D-G). In anaphase, the KIN-A rigor mutant failed to concentrate at the central spindle and
344 instead widely decorated the mitotic spindle, with increased signal observed at spindle poles possibly
345 due to poleward flux (Fig. 6, A-C). Expression of the KIN-A^{G209A} rigor mutant prevented Aurora B^{AUK1}
346 from translocating to the central spindle and caused lagging chromosomes (Figs. 6, D-F). The KIN-A
347 rigor mutation also slowed cell proliferation and caused accumulation of cells in anaphase (Figs. 6, G
348 and H). We conclude that central spindle localization of the CPC depends on KIN-A motor activity and
349 is required for proper chromosome segregation.
350
351
352 **Discussion**
353
354 Whereas astonishing diversity in kinetochore composition is seen among eukaryotes (Hooff et al.,
355 2017; Komaki et al., 2022; Tromer et al., 2019), the proteins of the regulatory circuitry underlying
356 chromosome segregation, such as the APC/C, SAC and CPC, are more widely conserved. Homologs of
357 the CPC proteins Aurora B kinase and its associated partner INCENP have been detected in almost all
358 sequenced eukaryotes, including kinetoplastids. The dynamic localization pattern exhibited by the CPC
359 (e.g. transferring from centromeres to the central spindle upon metaphase-anaphase transition) is
360 likewise highly conserved across eukaryotes but appears to be achieved through a variety of
361 mechanisms. For instance, while CPC recruitment to the centromeres in higher eukaryotes is governed
362 by two histone phosphorylation marks (Haspin-mediated H3T3ph and Bub1-mediated H2AT120ph),
363 budding yeasts employ a combination of histone modifications (Bub1-mediated H2AT121ph) and
364 kinetochore proteins as CPC receptors. Borealin^{Bir1} not only recognizes Sgo1 but also interacts with
365 the CBF3 complex through Ndc10 (Cho and Harrison, 2011; Yoon and Carbon, 1999). Furthermore,
366 INCENP^{Sli15}/Aurora B^{Ipl1} interact with the Ctf19 subunit of the COMA complex at kinetochores
367 (Fischböck-Halwachs et al., 2019). The proteins that form the localization module of the CPC in
368 different species appear to mirror the diversity in centromeric CPC receptors. In fact, many phyla lack

369 Borealin or Survivin homologs (Komaki et al., 2022). Komaki et al. recently identified two 'Survivin-
370 like' proteins, Borealin Related Interactor 1 and 2 (BORI1 and 2) as CPC proteins in *Arabidopsis*. Like
371 Survivin in other model eukaryotes, BORI1/2 engage in a triple helix bundle with INCENP and Borealin
372 but employ an FHA domain instead of a BIR domain to read H3T3ph (Komaki et al., 2022).

373 In this study, we have identified KIN-A and KIN-B as components of the CPC in trypanosomes,
374 and delineated a novel pathway for centromeric recruitment of the CPC in this evolutionary divergent
375 group of eukaryotes. In agreement with our work, an early study on the CPC in *T. brucei* found that
376 KIN-A and KIN-B co-purified with Aurora B^{AUK1}, $INCENP^{CPC1}$ and CPC2 based on a pull-down of an Aurora
377 B^{AUK1}-PTP fusion protein followed by mass spectrometry analysis (Li et al., 2008). However, HA-tagged
378 KIN-A and KIN-B were not detected at kinetochores (from late interphase until metaphase) nor at the
379 new FAZ tip (from late anaphase), and hence were not interpreted as CPC proteins. Contrary to this
380 report, our data clearly show that KIN-A and KIN-B are constitutive components of the CPC in *T. brucei*.
381 First, YFP-tagged KIN-A and KIN-B co-localize with Aurora B^{AUK1}, $INCENP^{CPC1}$ and CPC2 throughout the
382 cell cycle. Second, KIN-A and KIN-B are readily detected within native CPC complexes isolated by
383 immunoprecipitation of CPC subunits from cells arrested prior to anaphase and form robust crosslinks
384 with the other CPC subunits. Finally, YFP-Aurora B^{AUK1} and $INCENP^{CPC1}$-YFP are crucially dependent on
385 KIN-A and KIN-B for localizing both to metaphase kinetochores and to the anaphase central spindle.
386 Thus, the KIN-A:KIN-B subcomplex constitutes the localization module of the trypanosome CPC.

387 Biochemical, cell biological and in silico modelling approaches indicate that the kinesins KIN-
388 A and KIN-B form coiled coils between their central and C-terminal domains, respectively, which then
389 serve as a scaffold onto which $INCENP^{CPC1}$ and CPC2 assemble via their N-terminal α-helical domains.
390 The catalytic module of the trypanosomes CPC, consisting of Aurora B^{AUK1} bound to the C-terminal IN-
391 box of $INCENP^{CPC1}$, is connected to the KIN-A:KIN-B scaffold through a flexible linker in $INCENP^{CPC1}$.
392 While our on-beads cross-linking of native CPCs suggests that the catalytic module is positioned in
393 close proximity to the kinesin heads, this may not necessarily be true in vivo. For example, the catalytic
394 module may exist in both 'locked' and 'open' conformations with regard to its association with the
395 kinesin motor domains. We speculate that the interaction of the KIN-A motor domain with
396 microtubules from prometaphase onwards may cause the catalytic module to disengage from its
397 kinesin head-associated state. In analogy to the SAH domain of INCENP in other model eukaryotes
398 which has been proposed to function as a dog leash (Samejima et al., 2015; Santaguida and Musacchio,
399 2009), the $INCENP^{CPC1}$ flexible linker in trypanosomes may then permit Aurora B^{AUK1} to roam across a
400 larger but nevertheless spatially constrained target area to phosphorylate its substrates while still
401 being anchored to the kinetochore via KIN-A:KIN-B. Such models dealing with alternative
402 conformations of the CPC in various cellular context will require further testing in the future.

403 We propose that multiple weak interactions of the KIN-A C-terminal unstructured tail with
404 kinetochore components act in synergy to stabilize the CPC at kinetochores. Critically, these
405 interactions need to be of transient and reversible nature to permit the dynamic release of the CPC
406 upon anaphase onset. Three mechanisms are likely to play a role in this context. First, removal of the
407 KKT8 complex (the 'CD1 receptor') at the metaphase-anaphase transition effectively eliminates one
408 of the key CPC-kinetochore interfaces. Secondly, the affinity of the KIN-A C-terminal tail for its binding
409 partners at the kinetochore may be further finetuned through reversible post-translational
410 modifications. Interestingly, the KIN-A C-terminal tail is stuffed full of conserved CDK1^{CRK3} sites and is
411 also heavily phosphorylated by Aurora B^{AUK1} in vitro (data not shown), suggesting that the binding
412 properties the KIN-A C-terminus may be finely regulated. Finally, the high affinity of the N-terminal
413 motor domain of KIN-A for microtubules, coupled to the force generating ATP hydrolysis and plus-end
414 directed motion, eventually outcompetes the weakened interactions of the CPC with the kinetochore
415 and facilitates the extraction of the CPC from chromosomes onto spindle microtubules during
416 anaphase. Indeed, deletion of the KIN-A motor domain or impairment of its motor activity through N-
417 terminal GFP-NLS tagging causes the CPC to be trapped at kinetochores in anaphase. Central spindle
418 localization is additionally dependent on the ATPase activity of the KIN-A motor domain as illustrated
419 by the KIN-A rigor mutant. The exact details of how plus-end directed motion of KIN-A is achieved
420 remain to be investigated. Since KIN-B does not possess a functional kinesin motor domain, it is
421 unlikely that the KIN-A:KIN-B heterodimer moves hand-over-hand along microtubules as do
422 conventional (kinesin-1 family) kinesins. Rather, the KIN-A motor domain may function as a
423 monomeric unit and drive processive plus-end directed motion using a mechanism similar to kinesin-
424 3 family kinesins (such as KIF1A). Formation of transient complexes between the CPC and kinesins or
425 other microtubule plus-end tracking proteins upon anaphase onset appears to be a common theme
426 underlying the central spindle translocation of the CPC. For instance, the CPC interacts with MKLP2 or
427 Bim1^{EB1} in human and yeast cells, respectively (Gruneberg et al., 2004; Zimniak et al., 2012). Thus,
428 deeper understanding of the CPC regulation in trypanosomes is bound to provide evolutionary insights
429 into fundamental principles of chromosome segregation in eukaryotes and can lead to the discovery
430 of druggable targets to combat kinetoplastid diseases (Saldivia et al., 2020).
431
432
433 ## Materials and Methods
434
435 **Cloning**

436 All primers, plasmids, bacmids, and synthetic DNA used in this study as well as their source or
437 construction details are described in Supplemental Table S1. All constructs were sequence verified.
438
439 **Trypanosome culture**
440 All trypanosome cell lines used in this study were derived from *T. brucei* SmOxP927 procyclic form
441 cells (TREU 927/4 expressing T7 RNA polymerase and the tetracycline repressor to allow inducible
442 expression; Poon *et al.*, 2012) or from PCF1339 procyclic form cells (TREU 927/4 expressing T7 RNA
443 polymerase, tetracycline repressor and the Cas9 nuclease, Beneke et al., 2017) and are described in
444 Supplemental Table S1. Cells were grown at 28°C in SDM-79 medium supplemented with 10% (vol/vol)
445 heat-inactivated fetal calf serum, 7.5 µg/ml hemin (Brun and Schönenberger, 1979), and appropriate
446 selection drugs. Cell growth was monitored using a CASY cell counter (Roche). PCR products or
447 plasmids linearized by NotI were transfected into cells by electroporation (Biorad). Transfected cells
448 were selected by the addition of 30 µg/ml G418 (Sigma), 25 µg/ml hygromycin (Sigma), 5 µg/ml
449 phleomycin (Sigma), or 10 µg/ml blasticidin S (Insight biotechnology). To obtain endogenously tagged
450 clonal strains, transfected cells were selected by the addition of appropriate drugs and cloned by
451 dispensing dilutions into 96-well plates. Endogenous YFP tagging was performed using the pEnT5-Y
452 vector (Kelly et al., 2007) or a PCR-based method (Dean et al., 2015). Endogenous tdTomato tagging
453 was performed using pBA148 (Akiyoshi and Gull, 2014) and its derivatives. For doxycycline inducible
454 expression of head-to-head (pBA3-based) and hairpin (pBA310-based) RNAi constructs, GFP-NLS
455 (pBA310-based) and GFP-NLS-LacI fusion proteins (pBA795-based), the linearized plasmids were
456 integrated into 177-bp repeats on minichromosomes. Expression of GFP-NLS or GFP-NLS-LacI fusions
457 was induced by the addition of 10 ng/mL doxycycline for 24 h. RNAi was induced by the addition of 1
458 µg/ml doxycycline. LacO–LacI tethering experiments were carried out as described previously using
459 the LacO array inserted at the rDNA locus (Ishii and Akiyoshi, 2020; Landeira and Navarro, 2007).
460
461 **Immunoprecipitation followed by mass spectrometry (IP-MS)**
462 For standard IPs, 400-ml cultures of asynchronously growing cells were grown to ~5 – 10 million
463 cells/ml. Cells were pelleted by centrifugation (800 g, 10 min), washed once with PBS, and extracted
464 in PEME (100 mM Pipes-NaOH, pH 6.9, 2 mM EGTA, 1 mM $MgSO_4$, and 0.1 mM EDTA) with 1% NP-40,
465 protease inhibitors (10 µg/ml leupeptin, 10 µg/ml pepstatin, 10 µg/ml E-64, and 0.2 mM PMSF) and
466 phosphatase inhibitors (1 mM sodium pyrophosphate, 2 mM Na-β-glycerophosphate, 0.1 mM Na_3VO_4,
467 5 mM NaF, and 100 nM microcystin-LR) for 5 min at RT, followed by centrifugation at 1,800 g for 15
468 min. Samples were kept on ice from this point on. The pelleted fraction containing kinetochore
469 proteins was resuspended in modified buffer H (BH0.15: 25 mM Hepes, pH 8.0, 2 mM $MgCl_2$, 0.1 mM

470 EDTA, pH 8.0, 0.5 mM EGTA, pH 8.0, 1% NP-40, 150 mM KCl, and 15% glycerol) with protease and
471 phosphatase inhibitors. Samples were sonicated to solubilize kinetochore proteins (12 s, three times
472 with 1-min intervals on ice). 12 µg of mouse monoclonal anti-GFP antibodies (11814460001; Roche)
473 preconjugated with 60 µl slurry of Protein-G magnetic beads (10004D; Thermo Fisher Scientific) with
474 dimethyl pimelimidate (Unnikrishnan et al., 2012) were incubated with the extracts for 2.5 h with
475 constant rotation, followed by four washes with modified BH0.15 containing protease inhibitors,
476 phosphatase inhibitors and 2 mM DTT. Beads were further washed three times with pre-elution buffer
477 (50 mM Tris- HCl, pH 8.3, 75 mM KCl, and 1 mM EGTA). Bound proteins were eluted from the beads
478 by agitation in 60 µl of elution buffer (0.1% RapiGest [186001860; Waters] and 50 mM Tris-HCl, pH
479 8.3) for 25 min at RT. Eluates were then incubated at 100°C for 5 min. Proteins were reduced with 5
480 mM DTT at 37°C for 30 min and alkylated with 10 mM iodoacetamide at 37°C for 30 min. The reaction
481 was quenched by adding 10 mM DTT at 37°C for 30 min, and 100 µl of 20 mM Tris-HCl (pH 8.3) was
482 added. Proteins were digested overnight at 37°C with 0.2 µg trypsin (Promega). Formic acid was then
483 added to 2% and the samples were incubated at 37°C for 30 min to cleave RapiGest, followed by
484 centrifugation for 10 min. The supernatant was desalted over a C18 column and analyzed by
485 electrospray tandem mass spectrometry over a 60-min gradient using Q-Exactive (Thermo Fisher
486 Scientific) at the Advanced Proteomics Facility (University of Oxford). Peptides were identified by
487 searching tandem mass spectrometry spectra against the *T. brucei* protein database with MaxQuant
488 (version 2.0.1) with carbamidomethyl cysteine set as a fixed modification and oxidization (Met),
489 phosphorylation (Ser, Thr, and Tyr), and acetylation (Lys) set as variable modifications. Up to two
490 missed cleavages were allowed. The first peptide tolerance was set to 10 ppm. Results were filtered
491 to remove contaminants and reverse hits. Proteins identified with at least two peptides were
492 considered as significant and shown in Table S2 (protein FDR 1%).
493
494 **Ex vivo cross-linking of the native CPC and kinetochore complexes (IP-CLMS)**
495 For cross-linking IP-MS experiments, cell cultures were scaled up to 1,600 mL. Cell cultures were
496 treated with 10 µM MG132 for 4 h to enrich for cells in metaphase. Cell lysis and immunoprecipitation
497 steps were carried out as described above. After four washes with modified BH0.15 containing
498 protease inhibitors, phosphatase inhibitors and 2 mM DTT, beads were washed three times with 25
499 mM HEPES pH7.5, 150 mM NaCl. Proteins were then cross-linked on beads with 0.4 mM BS^3
500 (bis(sulfosuccinimidyl)suberate) (Thermo Fisher Scientific) for 30 min at RT with agitation, followed by
501 three washes in 25 mM HEPES pH7.5, 150 mM NaCl and a further three washes in 0.1 M ammonium
502 bicarbonate. Samples were then incubated in 8 M urea dissolved in 0.1 M ammonium bicarbonate for
503 10 min at RT with agitation. Proteins were reduced with 10 mM TCEP for 20 min and alkylated with 10

504 mM iodoacetamide for 40 min at RT. Proteins were then then pre-digested with 0.4 µg LysC for 2 h at
505 37°C. The urea concentration in the sample was brought down to < 1 M by addition of 0.1 M
506 ammonium bicarbonate before adding $CaCl_2$ (to 2 mM) and 0.7 µg of trypsin for overnight digestion
507 at 37°C. Formic acid was then added to 2% and the samples were frozen. The cross-linked samples
508 were further processed and analyzed at the proteomics core facility at EMBL Heidelberg. Digested
509 peptides were concentrated and desalted using an OASIS HLB µElution Plate (Waters) according to
510 manufacturer instructions. Crosslinked peptides were enriched using size exclusion chromatography
511 (Leitner et al., 2012). In brief, desalted peptides were reconstituted with SEC buffer (30% (v/v) ACN in
512 0.1% (v/v) TFA) and fractionated using a Superdex Peptide PC 3.2/30 column (GE) on a 1200 Infinity
513 HPLC system (Agilent) at a flow rate of 0.05 ml/min. Fractions eluting between 50-70 µl were
514 evaporated to dryness and reconstituted in 30 µl 4% (v/v) ACN in 1% (v/v) FA. Collected fractions were
515 analyzed by liquid chromatography (LC)-coupled tandem mass spectrometry (MS/MS) using an
516 UltiMate 3000 RSLC nano LC system (Dionex) fitted with a trapping cartridge (µ-Precolumn C18
517 PepMap 100, 5µm, 300 µm i.d. x 5 mm, 100 Å) and an analytical column (nanoEase M/Z HSS T3 column
518 75 µm x 250 mm C18, 1.8 µm, 100 Å, Waters). Trapping was carried out with a constant flow of
519 trapping solvent (0.05% trifluoroacetic acid in water) at 30 µl/min onto the trapping column for 6
520 minutes. Subsequently, peptides were eluted and separated on the analytical column using a gradient
521 composed of Solvent A (3% DMSO, 0.1% formic acid in water) and solvent B (3% DMSO, 0.1% formic
522 acid in acetonitrile) with a constant flow of 0.3 µl/min. The outlet of the analytical column was coupled
523 directly to an Orbitrap Fusion Lumos (Thermo Scientific, SanJose) mass spectrometer using the
524 nanoFlex source. The peptides were introduced into the Orbitrap Fusion Lumos via a Pico-Tip Emitter
525 360 µm OD x 20 µm ID; 10 µm tip (CoAnn Technologies) and an applied spray voltage of 2.1 kV,
526 instrument was operated in positive mode. The capillary temperature was set at 275°C. Only charge
527 states of 4-8 were included. The dynamic exclusion was set to 30 sec. and the intensity threshold was
528 $5e^4$. Full mass scans were acquired for a mass range 350-1700 m/z in profile mode in the orbitrap with
529 resolution of 120000. The AGC target was set to Standard and the injection time mode was set to
530 Auto. The instrument was operated in data dependent acquisition (DDA) mode with a cycle time of 3
531 sec between master scans and MSMS scans were acquired in the Orbitrap with a resolution of 30000,
532 with a fill time of up to 100 ms and a limitation of $2e^5$ ions (AGC target). A normalized collision energy
533 of 32 was applied. MS2 data was acquired in profile mode. RAW MS files were searched by the pLink2
534 software (Chen et al., 2019), with carbamidomethyl cysteine set as a fixed and oxidization (Met) set
535 as variable modifications. Up to two missed cleavages were allowed. Precursor tolerance was set to
536 10 ppm. All the identified cross-links are shown in Table S2 (FDR 5%). Cross-links were plotted using
537 xiView (Graham et al., 2019). All raw mass spectrometry files and custom database files used in this

538 study have been deposited with the ProteomeXchange Consortium via the PRIDE partner repository
539 (Deutsch et al., 2020; Perez-Riverol et al., 2019) with the dataset identifier PXD045987.
540
541 **Fluorescence microscopy**
542 Cells were washed once with PBS, settled onto glass slides, and fixed with 4% paraformaldehyde in
543 PBS for 5 min as described previously (Nerusheva and Akiyoshi, 2016). Cells were then permeabilized
544 with 0.1% NP-40 in PBS for 5 min and embedded in mounting media (1% wt/vol 1,4-
545 diazabicyclo[2.2.2]octane, 90% glycerol, 50 mM sodium phosphate, pH 8.0) containing 100 ng/ml
546 DAPI. Images were captured on a Zeiss Axioimager.Z2 microscope (Zeiss) installed with ZEN using a
547 Hamamatsu ORCA-Flash4.0 camera with 63× objective lenses (1.40 NA). Typically, ~20 optical slices
548 spaced 0.2 or 0.24 µm apart were collected. Images were analysed in ImageJ/Fiji (Schneider et al.,
549 2012). Kinetochore localization of endogenously tagged kinetochore proteins or ectopically expressed
550 constructs were examined manually by quantifying the number of cells that clearly had detectable
551 kinetochore-like dots at indicated cell cycle stages. Shown images are central slices.
552
553 **In silico structure and interaction predictions**
554 Structures and interactions were predicted with AlphaFold2-Multimer-v2 (Evans et al., 2022; Jumper
555 et al., 2021) through ColabFold version 1.3.0 using MMseqs2 (UniRef+Environmental) (Mirdita et al.,
556 2022). All structure figures were made using PyMOL version 2.5.2 (Schrödinger, LLC). The following
557 command was used to map pLDDT score onto the AF2 predicted structure models: spectrum b,
558 rainbow_rev, maximum=100, minimum=50.
559
560 **Protein purification from *E. coli***
561 Recombinant 6HIS-KKT8, KKT9, KKT11, KKT12 (pBA457) and derivatives were expressed in Rosetta
562 2(DE3)pLys *E. coli* cells (Novagen). 6HIS-KIN-A$^{2-309}$ (pBA2519) and 6HIS-KIN-B$^{2-316}$ (pBA2513) were
563 expressed in BL21(DE3) cells. Proteins were purified and eluted from TALON beads as previously
564 described (Llauró et al., 2018). Briefly, cells were grown in 2xTY media at 37°C to an OD_{600} of ~0.8, at
565 which point protein expression was induced by 0.1 mM IPTG, and then incubated overnight at 20°C.
566 Cells were pelleted at 3,400 g at 4°C and pellets were resuspended in P500 buffer (50 mM sodium
567 phosphate, pH 7.5, 500 mM NaCl, 5 mM imidazole and 10% glycerol) supplemented with protease
568 inhibitors (20 µg/ml leupeptin, 20 µg/ml pepstatin, 20 µg/ml E-64, 0.4 mM PMSF) and 1 mM TCEP,
569 and were sonicated on ice. Lysates were treated with benzonase nuclease (500 U/1 l culture) and spun
570 at 48,000 g at 4°C for 30 min. Supernatant was incubated with TALON beads (Takara Clontech) for 1 h
571 at 4°C, rotating. The beads were washed three times with lysis buffer and proteins were then eluted

572 with elution buffer (P500 buffer containing 250 mM imidazole with 1 mM TCEP). For microtubule co-
573 sedimentation assays, 6HIS-KIN-A$^{2-309}$ and 6HIS-KIN-B$^{2-316}$ were buffer exchanged into BRB80 (80 mM
574 Pipes-KOH, pH 6.9, 1 mM EGTA, and 1 mM $MgCl_2$) with 100 mM KCl using a Zeba columns (Thermo
575 Fisher) and flash-frozen in liquid nitrogen for -80°C storage. Polyacrylamide gels were stained with
576 SimplyBlue SafeStain (Invitrogen).
577
578 **Microtubule co-sedimentation assay**
579 Microtubule co-sedimentation assays were performed as described previously (Ludzia et al., 2021).
580 Briefly, taxol-stabilised microtubules were prepared by mixing 2.5 ml of 100 µM porcine tubulin
581 (Cytoskeleton) resuspended in BRB80 with 1 mM GTP (Cytoskeleton), 1.25 µl BRB80, 0.5 µl of 40 mM
582 $MgCl_2$, 0.5 µl of 10 mM GTP, and 0.25 µl DMSO, and incubated for 20 min at 37C. 120 ml of pre-
583 warmed BRB80 containing 12.5 µM Taxol (paclitaxel; Sigma) was added to the sample to bring the
584 microtubule concentration to ~2 µM. 20 µl of 6HIS-KIN-A$^{2-309}$ or 6HIS-KIN-B$^{2-316}$ (at final concentration
585 of 4 µM) in BRB80 with 100 mM KCl were mixed with 20 µl of microtubules (final, 1 µM) and incubated
586 for 45 min at room temperature. As a control, we incubated 6HIS-KIN-A$^{2-309}$ or 6HIS-KIN-B$^{2-316}$ with
587 BRB80 (with 12.5 µM Taxol). The samples were spun at 20,000 g at room temperature for 10 min, and
588 the supernatant was collected. To the tubes containing pelleted fractions, we added 40 µl of chilled
589 BRB80 with 5 mM $CaCl_2$ and incubated on ice for 5 min to depolymerise microtubules. Following the
590 incubation, samples were boiled for 5 min before SDS-PAGE. Gels were stained with SimplyBlue Safe
591 Stain (Invitrogen). Co-sedimentation assays were performed at least twice with similar results.
592
593 **Multiple sequence alignment**
594 Protein sequences and accession numbers for Aurora B^{AUK1}, INCENP^{CPC1}, CPC2, KIN-A and KIN-B used
595 in this study were retrieved from the TriTryp database (Aslett et al., 2010), UniProt (Bateman, 2019),
596 or a published study (Butenko et al., 2020). Searches for homologous proteins were done using BLAST
597 in the TriTryp database (Aslett et al., 2010) or using hmmsearch using manually prepared hmm profiles
598 (HMMER version 3.0; Eddy, 1998). Multiple sequence alignment was performed with MAFFT (L-INS-i
599 method, version 7) (Katoh et al., 2019) and visualised with the Clustalx colouring scheme in Jalview
600 (version 2.10) (Waterhouse et al., 2009).
601
602
603 ## Acknowledgements
604

605 We thank Miguel Navarro (Instituto de Parasitologıá y Biomedicina López-Neyra, Consejo Superior de
606 Investigaciones Cientificas, Spain) for providing pMig75 and pMig96 plasmids and Midori Ishii
607 Kanazawa and William Carter for helping trypanosome strain construction. We thank the Micron
608 Advanced Bioimaging Unit and the Advanced Proteomics Facility at the University of Oxford, and the
609 Proteomics Core Facility at the EMBL in Heidelberg, especially Mandy Rettel and Jennifer Schwarz, for
610 their support. We also thank Patryk Ludzia and Midori Ishii Kanazawa for comments on our
611 manuscript. D. Ballmer was supported by the Berrow Foundation. B. Akiyoshi was supported by a
612 Wellcome Trust Senior Research Fellowship (grant 210622/Z/18/Z).
613
614 The authors declare no competing financial interest.
615
616 Rights retention: This research was funded in whole or in part by Wellcome Trust (grant
617 210622/Z/18/Z). For the purpose of Open Access, the author has applied a CC BY public copyright
618 licence to any Author Accepted Manuscript (AAM) version arising from this submission.
619
620 Author contributions: D. Ballmer performed essentially all experiments except for some LacI/LacO
621 tethering experiments that were performed by B. Akiyoshi. D. Ballmer wrote the manuscript. B.
622 Akiyoshi edited the manuscript.
623
624

625 Figure legends

626

627 **Figure 1. KIN-A and KIN-B are bona fide CPC proteins in *T. brucei*.** (A) Heatmap showing enrichment
628 (log2 intensity based absolute quantification (IBAQ)) of the top 30 proteins, excluding ribosomal
629 proteins, co-purifying with YFP-Aurora B^{AUK1}. Cell line: BAP73. Immunoprecipitation was performed
630 using anti-GFP antibodies. See Table S2 for all proteins identified by mass spectrometry. (B) Cartoon
631 depicting the kinetoplast (K) / nucleus (N) configuration throughout the cell cycle in procyclic *T. brucei*,
632 with K* denoting an elongated kinetoplast. The kinetoplast is an organelle found uniquely in
633 kinetoplastids, which contains the mitochondrial DNA and replicates and segregates prior to nuclear
634 division. The KN configuration serves as a cell cycle marker (Siegel et al., 2008; Woodward and Gull,
635 1990). (C) to (E) Representative fluorescence micrographs showing the dynamic localization of YFP-
636 Aurora B^{AUK1} (C), KIN-A-YFP (D) and GFP-KIN-B (E) over the course of the cell cycle. Kinetochores are
637 marked with tdTomato-KKT2. DNA was stained with DAPI. Cell lines: BAP1515, BAP3066, BAP2288.
638 Scale bars, 2 µm.

639

640 **Figure 2. Kinetochore localization of the CPC depends on KIN-A.** (A) Representative fluorescence
641 micrographs showing the localization of YFP-tagged Aurora B^{AUK1}, $INCENP^{CPC1}$, KIN-A and KIN-B upon
642 RNAi-mediated knockdown of indicated CPC subunits. RNAi was induced with 1 µg/mL doxycycline for
643 24 h (KIN-B RNAi) or 16 h (all others). Cell lines: BAP3092, BAP2552, BAP2557, BAP3093, BAP2906,
644 BAP2900, BAP2904, BAP3094, BAP2899, BAP2893, BAP2897, BAP3095, BAP3096, BAP2560, BAP2564,
645 BAP3097. Scale bars, 2 µm. (B) to (E) Quantification of 2K1N cells that have kinetochore-like dots of
646 YFP-tagged Aurora B^{AUK1} (B), $INCENP^{CPC1}$ (C), KIN-A (D) and KIN-B (E) upon RNAi-mediated depletion of
647 indicated CPC components. All graphs depict the means (bar) ± SD of at least two replicates (shown as
648 dots). A minimum of 100 cells per replicate were quantified. * $P < 0.05$, ** $P \leq 0.01$, *** $P \leq 0.001$
649 (two-sided, unpaired t-test). (F) to (H) Representative fluorescence micrographs showing the
650 localization of ectopically expressed GFP-NLS-KIN-A^{fl} (F), -KIN-A^{2-309} (G) and -KIN-$A^{310-862}$ (H). Expression
651 of GFP-NLS fusion proteins was induced with 10 ng/mL doxycycline for 24 h. Kinetochores are marked
652 with tdTomato-KKT2. Arrowheads indicate KIN-A^{fl} and KIN-$A^{310-862}$ signals at kinetochores. KIN-A^{2-309} is
653 found at mitotic spindle during metaphase. Cell lines: BAP2286, BAP2297, BAP2287. Scale bars, 2 µm
654

655 **Figure 3. Structural model of the trypanosome CPC.** (A) Circular view of the BS^3 crosslinks observed
656 between the subunits of the trypanosome CPC, obtained from native complexes isolated by
657 immunoprecipitation of YFP-Aurora B^{AUK1} (Cell line: BAP2198b). pLink2 (Chen et al., 2019) was used to
658 obtain crosslinks from mass spectrometry data. xiView (Graham et al., 2019) was used for data
659 visualization. Only crosslinks with a score better than E^{-4} are shown. See Table S2 for all crosslinks
660 identified by mass spectrometry. (B) Cartoon representation of the trypanosome CPC, comprising
661 Aurora B^{AUK1} (crimson), $INCENP^{CPC1}$ (green), CPC2 (cyan), KIN-A^{1-599} (magenta) and KIN-B (yellow),
662 assembled from AlphaFold2 predictions shown in Figure S3. BS^3 crosslinks in (A) were mapped onto
663 the model using PyXlinkViewer (blue = distance constraints satisfied, red = distance constraints
664 violated, Cα-Cα Euclidean distance threshold = 30 Å).
665

666 **Figure 4. The CPC is recruited to kinetochores via the KKT7 – KKT8 complex pathway.** (A)
667 Representative fluorescence micrographs showing the localization of YFP-Aurora B^{AUK1} upon RNAi-
668 mediated knockdown of KKT7. RNAi was induced with 1 µg/mL doxycycline for 24 h. Cell line: BAP577.
669 Scale bars, 2 µm. (B) Quantification of 2K1N cells that have kinetochore-like dots of YFP-Aurora B^{AUK1}
670 upon knockdown of KKT7. All graphs depict the means (bar) ± SD of three replicates (shown as dots).
671 A minimum of 50 cells per replicate were quantified. *** $P \leq 0.001$ (two-sided, unpaired t-test). (C)
672 Representative fluorescence micrographs showing the localization of YFP-Aurora B^{AUK1} upon RNAi-

673 mediated knockdown of KKT9. RNAi was induced with 1 µg/mL doxycycline for 24 h. Kinetochores are
674 marked with tdTomato-KKT2. Cell line: BAP2276. Scale bars, 2 µm. (D) Quantification of 2K1N cells
675 that have kinetochore-like dots of YFP-Aurora B^{AUK1} upon knockdown of KKT9. All graphs depict the
676 means (bar) ± SD of three replicates (shown as dots). A minimum of 50 cells per replicate were
677 quantified. *** $P \leq 0.001$ (two-sided, unpaired t-test). (E) and (F) Representative micrographs of cells
678 in S phase and anaphase showing recruitment of tdTomato-Aurora B^{AUK1} to LacO foci marked by
679 ectopically expressed GFP-NLS-$KKT7^{2-261}$-LacI (E) or -KKT8-LacI (F). The insets show the magnification
680 of the boxed region. Expression of LacI fusion proteins was induced with 10 ng/mL doxycycline for 24
681 h. Arrowheads in (F) indicate anaphase kinetochore localization of GFP-NLS-KKT8-LacI and tdTomato-
682 Aurora B^{AUK1}. Anaphase kinetochore localization of tdTomato-Aurora B^{AUK1} was observed in 75% of
683 anaphase cells expressing GFP-NLS-KKT8-LacI (n = 28). Cell lines: BAP1395, BAP2640. Scale bars, 2 µm.
684 Of note, LacI fusions with $INCENP^{CPC1}$, KIN-A and KIN-B constructs robustly localized to kinetochores
685 like their endogenous counterparts and failed to form distinct LacI foci and could therefore not be
686 used to assess ectopic recruitment of KKT proteins. (G) Circular view of the BS^3 crosslinks observed
687 among KKT7 and KKT8 complex subunits, obtained from native complexes isolated by
688 immunoprecipitation of YFP-tagged KKIP1 (Cell line: BAP710a). pLink2 (Chen et al., 2019) was used to
689 obtain crosslinks from mass spectrometry data and xiView (Graham et al., 2019) was used for data
690 visualization. Only crosslinks with a score better than E^{-3} are shown. See Table S2 for all crosslinks
691 identified by mass spectrometry. (H) Indicated combinations of 6HIS-tagged KKT8, KKT9, KKT11 and
692 KKT12 were co-expressed in *E. coli*, followed by metal affinity chromatography and SDS-PAGE. I) Left:
693 AlphaFold2 model of the KKT7 – KKT8 complex, composed of $KKT7^{1-261}$ (green), KKT8 (blue), KKT12
694 (pink), KKT9 (cyan) and KKT11 (orange). BS^3 crosslinks in (G) were mapped onto the model using
695 PyXlinkViewer (blue = distance constraints satisfied, red = distance constraints violated, Cα-Cα
696 Euclidean distance threshold = 30 Å). Right: Predicted Aligned Error (PAE) plot of model shown on the
697 left (rank_1) and predicted IDDT per position for models rank_1 to rank_5. (J) Summary of the KKT7 –
698 KKT8 complex – CPC assembly pathway. Solid arrows indicate direct interactions as demonstrated by
699 crosslinking IP-MS.
700
701 **Figure 5. Two conserved domains within the C-terminal tail of KIN-A promote kinetochore**
702 **recruitment of the CPC.** (A) Left: AlphaFold2 model of KKT9:KKT11 in complex with KIN-$A^{700-862}$.
703 Cartoon representations of the proteins are coloured according to their pLDDT values (blue = high
704 confidence, red = low confidence). Right: Predicted Aligned Error (PAE) plot of model (rank_1)
705 predicted by AlphaFold2 (blue = high confidence, red = low confidence in the relative positions of the
706 domains to one another). CD1 of KIN-A was predicted to interact with KKT9:KKT11 in all five

707 AlphaFold2 models (rank_1 to rank_5). (B) Multiple sequence alignment of KIN-A CD1 and CD2
708 showing conservation. (C) to (E) Representative fluorescence micrographs showing the localization of
709 tdTomato-Aurora B^{AUK1} and YFP-tagged KIN-A^{wt} (C), KIN-$A^{\Delta CD1\ (717–743)}$ (D) and KIN-$A^{\Delta CD2\ (816–862)}$ (E). RNAi
710 was induced with 1 µg/mL doxycycline for 24 h to deplete the untagged KIN-A allele. Cell lines:
711 BAP3067, BAP3128, BAP3127. Scale bars, 2 µm. (F) Stacked bar charts showing the percentage of YFP-
712 tagged KIN-A^{wt}, KIN-$A^{\Delta CD1}$ and KIN-$A^{\Delta CD2}$ on kinetochores, kinetochores + spindle and spindle only in
713 metaphase cells. A minimum of 50 cells per condition were quantified. (G) Stacked bar charts showing
714 the percentage of tdTomato-Aurora B^{AUK1} on kinetochores, kinetochores + spindle and spindle only in
715 metaphase cells upon rescue with YFP-tagged KIN-A^{wt}, KIN-$A^{\Delta CD1}$ or KIN-$A^{\Delta CD2}$. A minimum of 50 cells
716 per condition were quantified. (H) Growth curves for indicated cell lines and conditions. RNAi was
717 induced with 1 µg/mL doxycycline for to deplete the untagged KIN-A allele in the knockdown
718 conditions and cultures were diluted at day 2. Cell lines: BAP3067, BAP3128, BAP3127.
719
720 **Figure 6. KIN-A motor activity is required for central spindle localization of the CPC in anaphase.** (A)
721 and (B) Representative fluorescence micrographs showing the localization of tdTomato-MAP103
722 (spindle marker) and YFP-tagged KIN-A^{wt} (A) or KIN-A^{G209A} (rigor mutant) (B). RNAi was induced with 1
723 µg/mL doxycycline for 24 h to deplete the untagged KIN-A allele. Cell lines: BAP3068, BAP3071. Scale
724 bars, 2 µm. (C) Quantification showing the percentage of anaphase cells that have YFP-tagged KIN-A^{wt}
725 or KIN-A^{G209A} localized at the central spindle. All graphs depict the means (bar) ± SD of three replicates
726 (shown as dots). A minimum of 40 cells per replicate were quantified. *** $P \leq 0.001$ (two-sided,
727 unpaired t-test). (D) and (E) Representative fluorescence micrographs showing the localization of
728 tdTomato-Aurora B^{AUK1} and YFP-tagged KIN-A^{wt} (D) or KIN-A^{G209A} (E). RNAi was induced with 1 µg/mL
729 doxycycline for 24 h to deplete the untagged KIN-A allele. Cell lines: BAP3067, BAP3070. Scale bars, 2
730 µm. (C) Quantification showing the percentage of anaphase cells that have tdTomato-Aurora B^{AUK1}
731 localized at the central spindle upon rescue with YFP-tagged KIN-A^{wt} or KIN-A^{G209A}. Graphs for the KIN-
732 A^{G209} rescue conditions (grey) depict the means (bar) ± SD of three replicates (shown as dots). A
733 minimum of 30 cells per replicate were quantified. (G) Growth curves for indicated cell lines and
734 conditions. RNAi was induced with 1 µg/mL doxycycline for to deplete the untagged KIN-A allele in the
735 knockdown conditions and cultures were diluted at day 2. Cell lines: BAP3064, BAP3065. (H) Cell cycle
736 profiles for the indicated cell lines and conditions. RNAi was induced with 1 µg/mL doxycycline to
737 deplete the untagged KIN-A allele in the knockdown conditions and cells were fixed after 24 h. All
738 graphs depict the means (bar) ± SD of at least two replicates. A minimum of 300 cells per replicate
739 were quantified. Cell lines: BAP3064, BAP3065. *** $P \leq 0.001$ (two-sided, unpaired t-test).
740

741 **Figure S1. KIN-A and KIN-B are bona fide CPC proteins in *T. brucei*.** (A) Clustered heatmap showing
742 enrichment (log2 intensity based absolute quantification (IBAQ)) of mitotic proteins co-purifying with
743 ectopically expressed GFP-NLS-INCENP^{CPC1}, GFP-NLS-KIN-A and GFP-NLS-KIN-B. The heatmap was
744 generated using the Python Seaborn library using WPGMA clustering. Cell lines: BAP2190, BAP2286,
745 BAP2288. See Table S2 for all proteins identified by mass spectrometry. (B) and (C) Representative
746 fluorescence micrographs showing the localization of tdTomato-Aurora B^{AUK1} and KIN-A-YFP (B) and
747 YFP-KIN-B (C) in late anaphase cells. Arrows indicate the population of CPC proteins localized to the
748 new FAZ tip. DNA was stained with DAPI. Cell lines: BAP3067, BAP2528. Scale bars, 2 µm. (D)
749 Phylogenetic tree of kinetoplastids, diplonemids and euglenids along with the presence (black dots) /
750 absence (white dots) patterns of CPC components. The phylogenetic tree of Euglenozoa is based on
751 (Butenko et al., 2020).
752
753 **Figure S2. Depletion of CPC proteins causes growth defects and cell cycle arrest.** (A) Growth curves
754 upon RNAi-mediated knockdown of indicated CPC subunits. Data are presented as the mean ± SD of
755 at least three replicates. RNAi was induced with 1 µg/mL doxycycline and cultures were diluted at day
756 2. CDS stands for coding sequence, UTR for untranslated region. Cell lines: BAP941, BAP2250,
757 BAP2251, BAP2252, BAP2253, BAP2557, BAP2558, BAP3076. (B) Cell cycle profiles upon knockdown
758 of indicated CPC subunits. RNAi was induced with 1 µg/mL doxycycline and cells were fixed at 16h (for
759 Aurora B^{AUK1}, INCENP^{CPC1} and KIN-A RNAi) or 24 h (CPC2 and KIN-B RNAi). All graphs depict the means
760 (bar) ± SD of at least two replicates. A minimum of 150 cells per replicate were quantified. Cell lines:
761 BAP2552, BAP3092, BAP2554, BAP2557, BAP3093. (C) Representative fluorescence micrographs
762 showing the localization of YFP-tagged Aurora B^{AUK1}, INCENP^{CPC1}, KIN-A and KIN-B upon RNAi-mediated
763 knockdown of CPC2. RNAi was induced with 1 µg/mL doxycycline for 24 h. Cell lines: BAP2554,
764 BAP2902, BAP2895, BAP2561. Scale bars, 2 µm. (D) Quantification of 2K1N cells that have kinetochore-
765 like dots of YFP-tagged Aurora B^{AUK1}, INCENP^{CPC1}, KIN-A or KIN-B upon knockdown of CPC2. All graphs
766 depict the means (bar) ± SD of at least two replicates (shown as dots). A minimum of 90 cells per
767 replicate were quantified. (E) to (G) Representative fluorescence micrographs showing the localization
768 of ectopically expressed GFP-NLS-KIN-B^{fl} (E), -KIN-B$^{2-316}$ (F) and -KIN-B$^{317-624}$ (G). Expression of GFP-NLS
769 fusion proteins was induced with 10 ng/mL doxycycline for 24 h. Kinetochores are marked with
770 tdTomato-KKT2. Cell lines: BAP2288, BAP2289, BAP2290. Scale bars, 2 µm.
771
772 **Figure S3. AlphaFold2 models of CPC subcomplexes and localization of CPC1 and CPC2 truncations.**
773 (A) to (D) Cartoon representations (rank_1 models) (left), PAE plots (center) and plDDT plots (right) of
774 AlphaFold2 predictions of indicated CPC subcomplexes. (E) to (J) Representative fluorescence

775 micrographs showing the localization of ectopically expressed GFP-NLS-INCENP$^{CPC1\ fl}$ (E), -INCENP$^{CPC1\ 2-}$
776 ^{147} (F), -INCENP$^{CPC1\ 2-147}$ (G), -CPC2^{fl} (H), -CPC2$^{2-120}$ (I) and -CPC2$^{121-250}$ (J) in different cell cycle stages.
777 Expression of GFP-NLS fusion proteins was induced with 10 ng/mL doxycycline for 24 h. Kinetochores
778 are marked with tdTomato-KKT2. Cell lines: BAP2190, BAP2191, BAP2193, BAP2194, BAP2195,
779 BAP2196. Scale bars, 2 µm.
780
781 **Figure S4. Kinetochore localization of Aurora B^{AUK1} and KIN-A depends on the KKT7 – KKT8 complex**
782 **pathway.** (A) Representative fluorescence micrographs showing the localization of YFP-Aurora B^{AUK1}
783 upon RNA-mediated knockdown of indicated KKT proteins. RNAi was induced with 1 µg/mL
784 doxycycline for 24 h. Cell lines: BAP3132, BAP576, BAP2551, BAP2550, BAP3133, BAP1019, BAP2549,
785 BAP2446. Scale bars, 2 µm. (B) Quantification of 2K1N cells that have kinetochore-like dots of YFP-
786 Aurora B^{AUK1} upon knockdown of indicated KKT proteins. A minimum of 40 cells per replicate were
787 examined. (C) Representative fluorescence micrographs showing the localization of KIN-A-YFP upon
788 RNA-mediated knockdown of KKT8 complex subunits. RNAi was induced with 1 µg/mL doxycycline for
789 24 h. Cell lines: BAP2970, BAP2968, BAP2969, BAP2971. Scale bars, 2 µm. (D) Quantification of 2K1N
790 cells that have kinetochore-like dots of KIN-A-YFP upon knockdown of indicated KKT8 complex
791 subunits. All graphs depict the means (bar) ± SD of at least two replicates (shown as dots). A minimum
792 of 50 cells per replicate were quantified. (E) Representative micrographs showing recruitment of
793 tdTomato-tagged KKT8, KKT9 and KKT12 to LacO foci marked by ectopically expressed GFP-NLS-KKT7^{2-}
794 ^{261}-LacI. Expression of GFP-NLS fusion proteins was induced with 10 ng/mL doxycycline for 24 h. Cell
795 lines: BAP871, BAP873, BAP874. Scale bars, 2 µm. (F) Representative fluorescence micrograph of an
796 anaphase cell showing localization of tdTomato-KKT8 and ectopically expressed GFP-NLS-KIN-A. The
797 insets show the magnification of the boxed region. Expression of GFP-NLS-KIN-A was induced with 10
798 ng/mL doxycycline for 24 h. Cell line: BAP3080. Scale bars, 2 µm. (G) Representative fluorescence
799 micrographs showing localization of YFP-tagged KKT8, KKT12 and KKT9 upon RNAi-mediated
800 knockdown of indicated KKT8 complex subunits. RNAi was induced with 1 µg/mL doxycycline for 24 h.
801 Cell lines: BAP2954, BAP2952, BAP2953, BAP2955, BAP2966, BAP2964, BAP2965, BAP2967, BAP2958,
802 BAP2956, BAP2957, BAP2959. Scale bars, 2 µm. (H) to (J) Quantification of 1K*1N and 2K1N cells that
803 have kinetochore-like dots of YFP-tagged KKT8 (H), KKT12 (I) and KKT9 (J) upon knockdown of
804 indicated KKT8 complex subunits. All graphs depict the means (bar) ± SD of at least three technical
805 replicates (shown as dots) from one experiment. A minimum of 100 cells per replicate were quantified.
806 ** $P \leq 0.01$, *** $P \leq 0.001$ (two-sided, unpaired t-test).
807

808 **Figure S5. CD1 and CD2 contribute synergistically to kinetochore localization of KIN-A.** (A) to (D)
809 Representative fluorescence micrographs showing the localization of ectopically expressed GFP-NLS-
810 KIN-A$^{310-862}$ (A), -KIN-A$^{310-862\ \Delta CD2}$ (B) and -KIN-B$^{310-862\ \Delta CD1}$ (C) and -KIN-A$^{310-716}$ (D). Expression of GFP-NLS
811 fusion proteins was induced with 10 ng/mL doxycycline for 24 h. Kinetochores are marked with
812 tdTomato-KKT2. Cell lines: BAP2287, BAP2948, BAP2949, BAP2947. Scale bars, 2 µm. (E)
813 Quantification of metaphase (left) and anaphase (right) cells that have kinetochore-like dots of
814 indicated GFP-NLS fusion proteins. All graphs depict the means (bar) ± SD of three replicates (shown
815 as dots). A minimum of 150 cells per replicate were quantified. *** $P \leq 0.001$ (two-sided, unpaired t-
816 test). (F) Stacked bar charts showing the percentage of KIN-A$^{\Delta CD1}$-YFP (left) or tdTomato-Aurora B^{AUK1}
817 (right) on kinetochores, kinetochores + spindle and spindle in KIN-A$^{\Delta CD1}$ metaphase cells with and
818 without KIN-A RNAi. A minimum of 70 cells per condition were quantified. Cell line: BAP3128. (G) Cell
819 cycle profiles for the indicated cell lines and conditions. RNAi was induced with 1 µg/mL doxycycline
820 to deplete the untagged KIN-A allele in the knockdown conditions and cells were fixed after 24 h. All
821 graphs depict the means (bar) ± SD of three replicates. A minimum of 500 cells per replicate were
822 quantified. Cell lines: BAP3067, BAP3127, BAP3128.
823
824 **Figure S6. Motor activity of KIN-A promotes kinetochore alignment at the metaphase plate.** (A)
825 Microtubule co-sedimentation assay with 6HIS-KIN-A$^{2-309}$ (upper) and 6HIS-KIN-B$^{2-316}$ (lower). (B) and
826 (C) Representative fluorescence micrographs showing localization of YFP-tagged KIN-A (B) and KIN-
827 A^{G209A} (rigor mutant) (C) in G2 and metaphase. Kinetochores are marked with tdTomato-KKT2. Cell
828 lines: BAP3066, BAP3069. Scale bars, 2 µm. (D) and (E) Upper: Representative fluorescence
829 micrographs showing localization of YFP-tagged KIN-A (D) and KIN-A^{G209A} (rigor mutant) (E) in
830 metaphase. The mitotic spindle is marked with tdTomato-MAP103. Bounding boxes indicate area used
831 for generation of intensity profiles in FIJI/Image J. Cell lines: BAP3068, BAP3071. Scale bars, 2 µm.
832 Lower: Example of 1D intensity profiles and corresponding heatmaps from the example cells shown
833 above. (F) and (G) Kinetochore alignment profiles for YFP-tagged KIN-A (F) and KIN-A^{G209A} (G). RNAi
834 was induced with 1 µg/mL doxycycline for 24 h to deplete the untagged KIN-A allele and cells were
835 treated with 10 µM MG132 for 4 h prior to fixing to prevent anaphase entry (Hayashi and Akiyoshi,
836 2018). WPGMA clustering was performed using the Python Seaborn library. Cell lines: BAP3064,
837 BAP3065.
838
839
840 **References**
841

842 Abad MA, Gupta T, Hadders MA, Meppelink A, Wopken JP, Blackburn E, Zou J, Gireesh A,
843 Buzuk L, Kelly DA, McHugh T, Rappsilber J, Lens SMA, Jeyaprakash AA. 2022.
844 Mechanistic basis for Sgo1-mediated centromere localization and function of the CPC.
845 *Journal of Cell Biology* **221**. doi:10.1083/JCB.202108156/213318
846 Adams RR, Maiato H, Earnshaw WC, Carmena M. 2001. Essential Roles of Drosophila Inner
847 Centromere Protein (Incenp) and Aurora B in Histone H3 Phosphorylation, Metaphase
848 Chromosome Alignment, Kinetochore Disjunction, and Chromosome Segregation.
849 *Journal of Cell Biology* **153**:865–880. doi:10.1083/JCB.153.4.865
850 Adams RR, Wheatleya SP, Gouldsworthy AM, Kandels-Lewis SE, Carmena M, Smythe C,
851 Gerloff DL, Earnshaw WC. 2000. INCENP binds the Aurora-related kinase AIRK2 and is
852 required to target it to chromosomes, the central spindle and cleavage furrow. *Current*
853 *Biology* **10**. doi:10.1016/S0960-9822(00)00673-4
854 Akiyoshi B. 2020. Analysis of a Mad2 homolog in Trypanosoma brucei provides possible
855 hints on the origin of the spindle checkpoint. *bioRxiv*.
856 Akiyoshi B, Gull K. 2014. Discovery of Unconventional Kinetochores in Kinetoplastids. *Cell*
857 **156**. doi:10.1016/j.cell.2014.01.049
858 Allshire RC, Karpen GH. 2008. Epigenetic regulation of centromeric chromatin: old dogs, new
859 tricks? *Nat Rev Genet* **9**. doi:10.1038/nrg2466
860 Aslett M, Aurrecoechea C, Berriman M, Brestelli J, Brunk BP, Carrington M, Depledge DP,
861 Fischer S, Gajria B, Gao X, Gardner MJ, Gingle A, Grant G, Harb OS, Heiges M, Hertz-
862 Fowler C, Houston R, Innamorato F, Iodice J, Kissinger JC, Kraemer E, Li W, Logan FJ,
863 Miller JA, Mitra S, Myler PJ, Nayak V, Pennington C, Phan I, Pinney DF, Ramasamy G,
864 Rogers MB, Roos DS, Ross C, Sivam D, Smith DF, Srinivasamoorthy G, Stoeckert CJ,
865 Subramanian S, Thibodeau R, Tivey A, Treatman C, Velarde G, Wang H. 2010.
866 TriTrypDB: a functional genomic resource for the Trypanosomatidae. *Nucleic Acids Res*
867 **38**. doi:10.1093/NAR/GKP851
868 Bateman A. 2019. UniProt: a worldwide hub of protein knowledge. *Nucleic Acids Res*
869 **47**:D506–D515. doi:10.1093/NAR/GKY1049
870 Beneke T, Madden R, Makin L, Valli J, Sunter J, Gluenz E. 2017. A CRISPR Cas9 high-
871 throughput genome editing toolkit for kinetoplastids. *R Soc Open Sci* **4**:1–16.
872 doi:10.1098/RSOS.170095
873 Berriman M. 2005. The Genome of the African Trypanosome Trypanosoma brucei. *Science*
874 *(1979)* **309**. doi:10.1126/science.1112642
875 Berriman M, Ghedin E, Hertz-Fowler C, Blandin G, Renauld H, Bartholomeu DC, Lennard NJ,
876 Caler E, Hamlin NE, Haas B, Böhme U, Hannick L, Aslett MA, Shallom J, Marcello L, Hou
877 L, Wickstead B, Alsmark UCM, Arrowsmith C, Atkin RJ, Barron AJ, Bringaud F, Brooks K,
878 Carrington M, Cherevach I, Chillingworth TJ, Churcher C, Clark LN, Corton CH, Cronin A,
879 Davies RM, Doggett J, Djikeng A, Feldblyum T, Field MC, Fraser A, Goodhead I, Hance Z,
880 Harper D, Harris BR, Hauser H, Hostetler J, Ivens A, Jagels K, Johnson D, Johnson J,
881 Jones K, Kerhornou AX, Koo H, Larke N, Landfear S, Larkin C, Leech V, Line A, Lord A,
882 MacLeod A, Mooney PJ, Moule S, Martin DMA, Morgan GW, Mungall K, Norbertczak H,
883 Ormond D, Pai G, Peacock CS, Peterson J, Quail MA, Rabbinowitsch E, Rajandream MA,
884 Reitter C, Salzberg SL, Sanders M, Schobel S, Sharp S, Simmonds M, Simpson AJ, Tallon
885 L, Turner CMR, Tait A, Tivey AR, Van Aken S, Walker D, Wanless D, Wang S, White B,
886 White O, Whitehead S, Woodward J, Wortman J, Adams MD, Embley TM, Gull K, Ullu E,
887 Barry JD, Fairlamb AH, Opperdoes F, Barrell BG, Donelson JE, Hall N, Fraser CM, Melville

SE, El-Sayed NM. 2005. The genome of the African trypanosome Trypanosoma brucei. *Science* **309**:416–422. doi:10.1126/SCIENCE.1112642

Bishop JD, Schumacher JM. 2002. Phosphorylation of the Carboxyl Terminus of Inner Centromere Protein (INCENP) by the Aurora B Kinase Stimulates Aurora B Kinase Activity. *Journal of Biological Chemistry* **277**. doi:10.1074/jbc.C200307200

Black BE, Cleveland DW. 2011. Epigenetic Centromere Propagation and the Nature of CENP-A Nucleosomes. *Cell* **144**. doi:10.1016/j.cell.2011.02.002

Broad AJ, DeLuca KF, DeLuca JG. 2020. Aurora B kinase is recruited to multiple discrete kinetochore and centromere regions in human cells. *J Cell Biol* **219**. doi:10.1083/JCB.201905144

Brun R, Schönenberger M. 1979. Cultivation and in vitro cloning or procyclic culture forms of Trypanosoma brucei in a semi-defined medium. *Acta Trop* **36**:289–292.

Butenko A, Opperdoes FR, Flegontova O, Horák A, Hampl V, Keeling P, Gawryluk RMR, Tikhonenkov D, Flegontov P, Lukeš J. 2020. Evolution of metabolic capabilities and molecular features of diplonemids, kinetoplastids, and euglenids. *BMC Biology 2020 18:1* **18**:1–28. doi:10.1186/S12915-020-0754-1

Campbell CS, Desai A. 2013. Tension sensing by Aurora B kinase is independent of survivin-based centromere localization. *Nature 2013 497:7447* **497**:118–121. doi:10.1038/nature12057

Carmena M, Wheelock M, Funabiki H, Earnshaw WC. 2012. The chromosomal passenger complex (CPC): from easy rider to the godfather of mitosis. *Nat Rev Mol Cell Biol* **13**. doi:10.1038/nrm3474

Cavalier-Smith T. 2010. Kingdoms Protozoa and Chromista and the eozoan root of the eukaryotic tree. *Biol Lett* **6**:342–345. doi:10.1098/RSBL.2009.0948

Cheeseman IM, Chappie JS, Wilson-Kubalek EM, Desai A. 2006. The Conserved KMN Network Constitutes the Core Microtubule-Binding Site of the Kinetochore. *Cell* **127**. doi:10.1016/j.cell.2006.09.039

Chen ZL, Meng JM, Cao Y, Yin JL, Fang RQ, Fan SB, Liu C, Zeng WF, Ding YH, Tan D, Wu L, Zhou WJ, Chi H, Sun RX, Dong MQ, He SM. 2019. A high-speed search engine pLink 2 with systematic evaluation for proteome-scale identification of cross-linked peptides. *Nature Communications 2019 10:1* **10**:1–12. doi:10.1038/s41467-019-11337-z

Cho US, Harrison SC. 2011. Ndc10 is a platform for inner kinetochore assembly in budding yeast. *Nat Struct Mol Biol* **19**:48–56. doi:10.1038/NSMB.2178

Cooke CA, Heck MMS, Earnshaw WC. 1987. The inner centromere protein (INCENP) antigens: movement from inner centromere to midbody during mitosis. *J Cell Biol* **105**:2053–2067. doi:10.1083/JCB.105.5.2053

D'Archivio S, Wickstead B. 2017. Trypanosome outer kinetochore proteins suggest conservation of chromosome segregation machinery across eukaryotes. *Journal of Cell Biology* **216**. doi:10.1083/jcb.201608043

Dean S, Sunter J, Wheeler RJ, Hodkinson I, Gluenz E, Gull K. 2015. A toolkit enabling efficient, scalable and reproducible gene tagging in trypanosomatids. *Open Biol* **5**. doi:10.1098/RSOB.140197

Deutsch EW, Bandeira N, Sharma V, Perez-Riverol Y, Carver JJ, Kundu DJ, García-Seisdedos D, Jarnuczak AF, Hewapathirana S, Pullman BS, Wertz J, Sun Z, Kawano S, Okuda S, Watanabe Y, Hermjakob H, Maclean B, Maccoss MJ, Zhu Y, Ishihama Y, Vizcaíno JA. 2020. The ProteomeXchange consortium in 2020: enabling 'big data' approaches in proteomics. *Nucleic Acids Res* **48**:D1145. doi:10.1093/NAR/GKZ984

935 Drinnenberg IA, Akiyoshi B. 2017. Evolutionary Lessons from Species with Unique
936 Kinetochores. *Prog Mol Subcell Biol* **56**:111–138. doi:10.1007/978-3-319-58592-
937 5_5/TABLES/1
938 Eddy SR. 1998. Profile hidden Markov models. *Bioinformatics* **14**:755–763.
939 doi:10.1093/BIOINFORMATICS/14.9.755
940 Evans R, O'neill M, Pritzel A, Antropova N, Senior A, Green T, Žídek A, Bates R, Blackwell S,
941 Yim J, Ronneberger O, Bodenstein S, Zielinski M, Bridgland A, Potapenko A, Cowie A,
942 Tunyasuvunakool K, Jain R, Clancy E, Kohli P, Jumper J, Hassabis D. 2022. Protein
943 complex prediction with AlphaFold-Multimer. doi:10.1101/2021.10.04.463034
944 Fischböck-Halwachs J, Singh S, Potocnjak M, Hagemann G, Solis-Mezarino V, Woike S,
945 Ghodgaonkar-Steger M, Weissmann F, Gallego LD, Rojas J, Andreani J, Köhler A, Herzog
946 F. 2019. The COMA complex interacts with Cse4 and positions Sli15/Ipl1 at the budding
947 yeast inner kinetochore. *Elife* **8**. doi:10.7554/ELIFE.42879
948 Foltz DR, Jansen LET, Black BE, Bailey AO, Yates JR, Cleveland DW. 2006. The human CENP-A
949 centromeric nucleosome-associated complex. *Nat Cell Biol* **8**. doi:10.1038/ncb1397
950 García-Rodríguez LJ, Kasciukovic T, Denninger V, Tanaka TU. 2019. Aurora B-INCENP
951 Localization at Centromeres/Inner Kinetochores Is Required for Chromosome Bi-
952 orientation in Budding Yeast. *Current Biology* **29**:1536-1544.e4.
953 doi:10.1016/J.CUB.2019.03.051
954 Gassmann R, Carvalho A, Henzing AJ, Ruchaud S, Hudson DF, Honda R, Nigg EA, Gerloff DL,
955 Earnshaw WC. 2004. Borealin: a novel chromosomal passenger required for stability of
956 the bipolar mitotic spindle. *Journal of Cell Biology* **166**. doi:10.1083/jcb.200404001
957 Graham M, Combe C, Kolbowski L, Rappsilber J. 2019. xiView: A common platform for the
958 downstream analysis of Crosslinking Mass Spectrometry data. *bioRxiv* 561829.
959 doi:10.1101/561829
960 Gruneberg U, Neef R, Honda R, Nigg EA, Barr FA. 2004. Relocation of Aurora B from
961 centromeres to the central spindle at the metaphase to anaphase transition requires
962 MKlp2. *J Cell Biol* **166**:167–172. doi:10.1083/JCB.200403084
963 Hadders MA, Hindriksen S, Truong MA, Mhaskar AN, Pepijn Wopken J, Vromans MJM, Lens
964 SMA. 2020. Untangling the contribution of Haspin and Bub1 to Aurora B function
965 during mitosis. *Journal of Cell Biology* **219**. doi:10.1083/JCB.201907087/133700
966 Hayashi H, Akiyoshi B. 2018. Degradation of cyclin B is critical for nuclear division in
967 *Trypanosoma brucei*. *Biol Open*. doi:10.1242/bio.031609
968 Hochegger H, Hégarat N, Pereira-Leal JB. 2012. Aurora at the pole and equator: overlapping
969 functions of Aurora kinases in the mitotic spindle. *Open Biol* **3**.
970 doi:10.1098/RSOB.120185
971 Hooff JJ, Tromer E, Wijk LM, Snel B, Kops GJ. 2017. Evolutionary dynamics of the
972 kinetochore network in eukaryotes as revealed by comparative genomics. *EMBO Rep*
973 **18**. doi:10.15252/embr.201744102
974 Hori T, Fukagawa T. 2012. Establishment of the vertebrate kinetochores. *Chromosome*
975 *Research* **20**. doi:10.1007/s10577-012-9289-9
976 Hu H, Yu Z, Liu Y, Wang T, Wei Y, Li Z. 2014. The Aurora B kinase in *Trypanosoma brucei*
977 undergoes post-translational modifications and is targeted to various subcellular
978 locations through binding to TbCPC1. *Mol Microbiol* **91**. doi:10.1111/mmi.12458
979 Hümmer S, Mayer TU. 2009. Cdk1 Negatively Regulates Midzone Localization of the Mitotic
980 Kinesin Mklp2 and the Chromosomal Passenger Complex. *Current Biology* **19**:607–612.
981 doi:10.1016/J.CUB.2009.02.046

982 Integrating Neglected Tropical Diseases into Global Health and Development: Fourth World
983 Health Organization Report on Neglected Tropical Diseases (WHO, 2017). 2017.
984 Ishii M, Akiyoshi B. 2020. Characterization of unconventional kinetochore kinases KKT10/19
985 in *Trypanosoma brucei*. *J Cell Sci*. doi:10.1242/jcs.240978
986 Izuta H, Ikeno M, Suzuki N, Tomonaga T, Nozaki N, Obuse C, Kisu Y, Goshima N, Nomura F,
987 Nomura N, Yoda K. 2006. Comprehensive analysis of the ICEN (Interphase Centromere
988 Complex) components enriched in the CENP-A chromatin of human cells. *Genes to Cells*
989 **11**. doi:10.1111/j.1365-2443.2006.00969.x
990 Je Van Hooff J, Tromer E, Van Wijk LM, Snel B, Geert &, Kops J. 2017. Evolutionary dynamics
991 of the kinetochore network in eukaryotes as revealed by comparative genomics. *EMBO*
992 *Rep* **18**:1559–1571. doi:10.15252/EMBR.201744102
993 Jeyaprakash AA, Basquin C, Jayachandran U, Conti E. 2011. Structural Basis for the
994 Recognition of Phosphorylated Histone H3 by the Survivin Subunit of the Chromosomal
995 Passenger Complex. *Structure* **19**:1625–1634. doi:10.1016/J.STR.2011.09.002
996 Jeyaprakash AA, Klein UR, Lindner D, Ebert J, Nigg EA, Conti E. 2007. Structure of a Survivin–
997 Borealin–INCENP Core Complex Reveals How Chromosomal Passengers Travel
998 Together. *Cell* **131**. doi:10.1016/j.cell.2007.07.045
999 Jumper J, Evans R, Pritzel A, Green T, Figurnov M, Ronneberger O, Tunyasuvunakool K, Bates
1000 R, Žídek A, Potapenko A, Bridgland A, Meyer C, Kohl SAA, Ballard AJ, Cowie A, Romera-
1001 Paredes B, Nikolov S, Jain R, Adler J, Back T, Petersen S, Reiman D, Clancy E, Zielinski M,
1002 Steinegger M, Pacholska M, Berghammer T, Bodenstein S, Silver D, Vinyals O, Senior
1003 AW, Kavukcuoglu K, Kohli P, Hassabis D. 2021. Highly accurate protein structure
1004 prediction with AlphaFold. *Nature 2021 596:7873* **596**:583–589. doi:10.1038/s41586-
1005 021-03819-2
1006 Katoh K, Rozewicki J, Yamada KD. 2019. MAFFT online service: multiple sequence alignment,
1007 interactive sequence choice and visualization. *Brief Bioinform* **20**:1160–1166.
1008 doi:10.1093/BIB/BBX108
1009 Kawashima SA, Yamagishi Y, Honda T, Lshiguro KI, Watanabe Y. 2010. Phosphorylation of
1010 H2A by Bub1 prevents chromosomal instability through localizing shugoshin. *Science*
1011 *(1979)* **327**:172–177. doi:10.1126/SCIENCE.1180189/SUPPL_FILE/KAWASHIMA-
1012 SOM.REVISION.1.PDF
1013 Kelly AE, Ghenoiu C, Xue JZ, Zierhut C, Kimura H, Funabiki H. 2010. Survivin reads
1014 phosphorylated histone H3 threonine 3 to activate the mitotic kinase Aurora B. *Science*
1015 **330**:235–239. doi:10.1126/SCIENCE.1189505
1016 Kelly S, Reed J, Kramer S, Ellis L, Webb H, Sunter J, Salje J, Marinsek N, Gull K, Wickstead B,
1017 Carrington M. 2007. Functional genomics in Trypanosoma brucei: A collection of
1018 vectors for the expression of tagged proteins from endogenous and ectopic gene loci.
1019 *Mol Biochem Parasitol* **154**. doi:10.1016/j.molbiopara.2007.03.012
1020 Kitagawa M, Fung SYS, Hameed UFS, Goto H, Inagaki M, Lee SH. 2014. Cdk1 coordinates
1021 timely activation of MKlp2 kinesin with relocation of the chromosome passenger
1022 complex for cytokinesis. *Cell Rep* **7**:166–179. doi:10.1016/J.CELREP.2014.02.034
1023 Klein UR, Nigg EA, Gruneberg U. 2006. Centromere targeting of the chromosomal passenger
1024 complex requires a ternary subcomplex of Borealin, Survivin, and the N-terminal
1025 domain of INCENP. *Mol Biol Cell* **17**:2547–2558. doi:10.1091/MBC.E05-12-1133
1026 Komaki S, Tromer EC, De Jaeger G, De Winne N, Heese M, Schnittger A. 2022. Molecular
1027 convergence by differential domain acquisition is a hallmark of chromosomal

1028 passenger complex evolution. *Proc Natl Acad Sci U S A* **119**.
1029 doi:10.1073/PNAS.2200108119/-/DCSUPPLEMENTAL
1030 Krenn V, Musacchio A. 2015. The Aurora B Kinase in Chromosome Bi-Orientation and
1031 Spindle Checkpoint Signaling. *Front Oncol* **5**. doi:10.3389/FONC.2015.00225
1032 Landeira D, Navarro M. 2007. Nuclear repositioning of the VSG promoter during
1033 developmental silencing in Trypanosoma brucei. *Journal of Cell Biology* **176**.
1034 doi:10.1083/jcb.200607174
1035 Leitner A, Reischl R, Walzthoeni T, Herzog F, Bohn S, Förster F, Aebersold R. 2012. Expanding
1036 the chemical cross-linking toolbox by the use of multiple proteases and enrichment by
1037 size exclusion chromatography. *Mol Cell Proteomics* **11**.
1038 doi:10.1074/MCP.M111.014126
1039 Li Z, Lee JH, Chu F, Burlingame AL, Günzl A, Wang CC. 2008. Identification of a Novel
1040 Chromosomal Passenger Complex and Its Unique Localization during Cytokinesis in
1041 Trypanosoma brucei. *PLoS One* **3**. doi:10.1371/journal.pone.0002354
1042 Liang C, Zhang Z, Chen Q, Yan H, Zhang M, Zhou L, Xu J, Lu W, Wang F. 2020. Centromere-
1043 localized Aurora B kinase is required for the fidelity of chromosome segregation. *J Cell*
1044 *Biol* **219**. doi:10.1083/JCB.201907092
1045 Llauró A, Hayashi H, Bailey ME, Wilson A, Ludzia P, Asbury CL, Akiyoshi B. 2018. The
1046 kinetoplastid kinetochore protein KKT4 is an unconventional microtubule tip–coupling
1047 protein. *Journal of Cell Biology* **217**. doi:10.1083/jcb.201711181
1048 Lowell JE, Cross GAM. 2004. A variant histone H3 is enriched at telomeres in Trypanosoma
1049 brucei. *J Cell Sci* **117**:5937–5947. doi:10.1242/JCS.01515
1050 Ludzia P, Lowe ED, Marcianò G, Mohammed S, Redfield C, Akiyoshi B. 2021. Structural
1051 characterization of KKT4, an unconventional microtubule-binding kinetochore protein.
1052 *Structure* **29**:1014-1028.e8. doi:10.1016/J.STR.2021.04.004
1053 Maddox PS, Corbett KD, Desai A. 2012. Structure, assembly and reading of centromeric
1054 chromatin. *Curr Opin Genet Dev* **22**. doi:10.1016/j.gde.2011.11.005
1055 Marcianò G, Ishii M, Nerusheva OO, Akiyoshi B. 2021. Kinetoplastid kinetochore proteins
1056 KKT2 and KKT3 have unique centromere localization domains. *J Cell Biol* **220**.
1057 doi:10.1083/JCB.202101022
1058 Meraldi P, McAinsh AD, Rheinbay E, Sorger PK. 2006. Phylogenetic and structural analysis of
1059 centromeric DNA and kinetochore proteins. *Genome Biol* **7**:1–21. doi:10.1186/GB-
1060 2006-7-3-R23/FIGURES/11
1061 Mirdita M, Schütze K, Moriwaki Y, Heo L, Ovchinnikov S, Steinegger M. 2022. ColabFold:
1062 making protein folding accessible to all. *Nature Methods 2022 19:6* **19**:679–682.
1063 doi:10.1038/s41592-022-01488-1
1064 Nerusheva OO, Akiyoshi B. 2016. Divergent polo box domains underpin the unique
1065 kinetoplastid kinetochore. *Open Biol* **6**. doi:10.1098/rsob.150206
1066 Nerusheva OO, Ludzia P, Akiyoshi B. 2019. Identification of four unconventional
1067 kinetoplastid kinetochore proteins KKT22–25 in *Trypanosoma brucei*. *Open Biol* **9**.
1068 doi:10.1098/rsob.190236
1069 Okada M, Cheeseman IM, Hori T, Okawa K, McLeod IX, Yates JR, Desai A, Fukagawa T. 2006.
1070 The CENP-H–I complex is required for the efficient incorporation of newly synthesized
1071 CENP-A into centromeres. *Nat Cell Biol* **8**. doi:10.1038/ncb1396
1072 Perez-Riverol Y, Csordas A, Bai J, Bernal-Llinares M, Hewapathirana S, Kundu DJ, Inuganti A,
1073 Griss J, Mayer G, Eisenacher M, Pérez E, Uszkoreit J, Pfeuffer J, Sachsenberg T, Yilmaz Ş,
1074 Tiwary S, Cox J, Audain E, Walzer M, Jarnuczak AF, Ternent T, Brazma A, Vizcaíno JA.

1075 2019. The PRIDE database and related tools and resources in 2019: improving support
1076 for quantification data. *Nucleic Acids Res* **47**:D442–D450. doi:10.1093/NAR/GKY1106
1077 Romano A, Guse A, Krascenicova I, Schnabel H, Schnabel R, Glotzer M. 2003. CSC-1: a
1078 subunit of the Aurora B kinase complex that binds to the survivin-like protein BIR-1 and
1079 the incenp-like protein ICP-1. *Journal of Cell Biology* **161**. doi:10.1083/jcb.200207117
1080 Saldivia M, Fang E, Ma X, Myburgh E, Carnielli JBT, Bower-Lepts C, Brown E, Ritchie R,
1081 Lakshminarayana SB, Chen Y-L, Patra D, Ornelas E, Koh HXY, Williams SL, Supek F,
1082 Paape D, McCulloch R, Kaiser M, Barrett MP, Jiricek J, Diagana TT, Mottram JC, Rao SPS.
1083 2020. Targeting the trypanosome kinetochore with CLK1 protein kinase inhibitors. *Nat*
1084 *Microbiol* **5**:1207–1216. doi:10.1038/s41564-020-0745-6
1085 Samejima K, Platani M, Wolny M, Ogawa H, Vargiu G, Knight PJ, Peckham M, Earnshaw WC.
1086 2015. The Inner Centromere Protein (INCENP) Coil Is a Single α-Helix (SAH) Domain
1087 That Binds Directly to Microtubules and Is Important for Chromosome Passenger
1088 Complex (CPC) Localization and Function in Mitosis. *J Biol Chem* **290**:21460–21472.
1089 doi:10.1074/JBC.M115.645317
1090 Sampath SC, Ohi R, Leismann O, Salic A, Pozniakovski A, Funabiki H. 2004. The Chromosomal
1091 Passenger Complex Is Required for Chromatin-Induced Microtubule Stabilization and
1092 Spindle Assembly. *Cell* **118**. doi:10.1016/j.cell.2004.06.026
1093 Santaguida S, Musacchio A. 2009. The life and miracles of kinetochores. *EMBO J* **28**:2511–
1094 2531. doi:10.1038/EMBOJ.2009.173
1095 Schiffrin B, Radford SE, Brockwell DJ, Calabrese AN. 2020. PyXlinkViewer: A flexible tool for
1096 visualization of protein chemical crosslinking data within the PyMOL molecular graphics
1097 system. *Protein Sci* **29**:1851–1857. doi:10.1002/PRO.3902
1098 Schneider CA, Rasband WS, Eliceiri KW. 2012. NIH Image to ImageJ: 25 years of image
1099 analysis. *Nature Methods 2012 9:7* **9**:671–675. doi:10.1038/nmeth.2089
1100 Serena M, Bastos RN, Elliott PR, Barr FA. 2020. Molecular basis of MKLP2-dependent Aurora
1101 B transport from chromatin to the anaphase central spindle. *Journal of Cell Biology* **219**.
1102 doi:10.1083/JCB.201910059/151730
1103 Siegel TN, Hekstra DR, Cross GAM. 2008. Analysis of the Trypanosoma brucei cell cycle by
1104 quantitative DAPI imaging. *Mol Biochem Parasitol* **160**.
1105 doi:10.1016/j.molbiopara.2008.04.004
1106 Stuart K, Brun R, Croft S, Fairlamb A, Gürtler RE, McKerrow J, Reed S, Tarleton R. 2008.
1107 Kinetoplastids: related protozoan pathogens, different diseases. *Journal of Clinical*
1108 *Investigation* **118**. doi:10.1172/JCI33945
1109 Trivedi P, Stukenberg PT. 2016. A centromere-signaling network underlies the coordination
1110 among mitotic events. *Trends Biochem Sci* **41**:160. doi:10.1016/J.TIBS.2015.11.002
1111 Tromer EC, van Hooff JJE, Kops GJPL, Snel B. 2019. Mosaic origin of the eukaryotic
1112 kinetochore. *Proc Natl Acad Sci U S A* **116**:12873–12882.
1113 doi:10.1073/PNAS.1821945116/SUPPL_FILE/PNAS.1821945116.SD05.XLSX
1114 Tsukahara T, Tanno Y, Watanabe Y. 2010. Phosphorylation of the CPC by Cdk1 promotes
1115 chromosome bi-orientation. *Nature 2010 467:7316* **467**:719–723.
1116 doi:10.1038/nature09390
1117 Tu X, Kumar P, Li Z, Wang CC. 2006. An Aurora Kinase Homologue Is Involved in Regulating
1118 Both Mitosis and Cytokinesis in Trypanosoma brucei. *Journal of Biological Chemistry*
1119 **281**. doi:10.1074/jbc.M511504200

1120 Unnikrishnan A, Akiyoshi B, Biggins S, Tsukiyama T. 2012. An Efficient Purification System for
1121 Native Minichromosome from Saccharomyces cerevisiae. doi:10.1007/978-1-61779-
1122 477-3_8
1123 Vader G, Kauw JJW, Medema RH, Lens SMA. 2006. Survivin mediates targeting of the
1124 chromosomal passenger complex to the centromere and midbody. *EMBO Rep* **7**.
1125 doi:10.1038/sj.embor.7400562
1126 Van Der Lee R, Buljan M, Lang B, Weatheritt RJ, Daughdrill GW, Dunker AK, Fuxreiter M,
1127 Gough J, Gsponer J, Jones DT, Kim PM, Kriwacki RW, Oldfield CJ, Pappu R V., Tompa P,
1128 Uversky VN, Wright PE, Babu MM. 2014. Classification of intrinsically disordered
1129 regions and proteins. *Chem Rev* **114**:6589–6631.
1130 doi:10.1021/CR400525M/ASSET/IMAGES/LARGE/CR-2013-00525M_0006.JPEG
1131 Wang F, Dai J, Daum JR, Niedzialkowska E, Banerjee B, Stukenberg PT, Gorbsky GJ, Higgins
1132 JMG. 2010. Histone H3 Thr-3 phosphorylation by Haspin positions Aurora B at
1133 centromeres in mitosis. *Science* **330**:231–235. doi:10.1126/SCIENCE.1189435
1134 Waterhouse AM, Procter JB, Martin DMA, Clamp M, Barton GJ. 2009. Jalview Version 2--a
1135 multiple sequence alignment editor and analysis workbench. *Bioinformatics* **25**:1189–
1136 1191. doi:10.1093/BIOINFORMATICS/BTP033
1137 Westhorpe FG, Straight AF. 2013. Functions of the centromere and kinetochore in
1138 chromosome segregation. *Curr Opin Cell Biol* **25**. doi:10.1016/j.ceb.2013.02.001
1139 Wheatley SP, Carvalho A, Vagnarelli P, Earnshaw WC. 2001. INCENP is required for proper
1140 targeting of Survivin to the centromeres and the anaphase spindle during mitosis.
1141 *Current Biology* **11**. doi:10.1016/S0960-9822(01)00238-X
1142 Wickstead B, Gull K. 2006. A “Holistic” Kinesin Phylogeny Reveals New Kinesin Families and
1143 Predicts Protein Functions □ D. *Mol Biol Cell* **17**:1734–1743. doi:10.1091/mbc.E05-11-
1144 1090
1145 Woodward R, Gull K. 1990. Timing of nuclear and kinetoplast DNA replication and early
1146 morphological events in the cell cycle of Trypanosoma brucei. *J Cell Sci* **95**.
1147 doi:10.1242/jcs.95.1.49
1148 Yamagishi Y, Honda T, Tanno Y, Watanabe Y. 2010. Two histone marks establish the inner
1149 centromere and chromosome bi-orientation. *Science* **330**:239–243.
1150 doi:10.1126/SCIENCE.1194498
1151 Yoon HJ, Carbon J. 1999. Participation of Bir1p, a member of the inhibitor of apoptosis
1152 family, in yeast chromosome segregation events. *Proc Natl Acad Sci U S A* **96**:13208–
1153 13213. doi:10.1073/PNAS.96.23.13208
1154 Zimniak T, Fitz V, Zhou H, Lampert F, Opravil S, Mechtler K, Stolt-Bergner P, Westermann S.
1155 2012. Spatiotemporal regulation of Ipl1/Aurora activity by direct Cdk1 phosphorylation.
1156 *Curr Biol* **22**:787–793. doi:10.1016/J.CUB.2012.03.007
1157

Figure 1

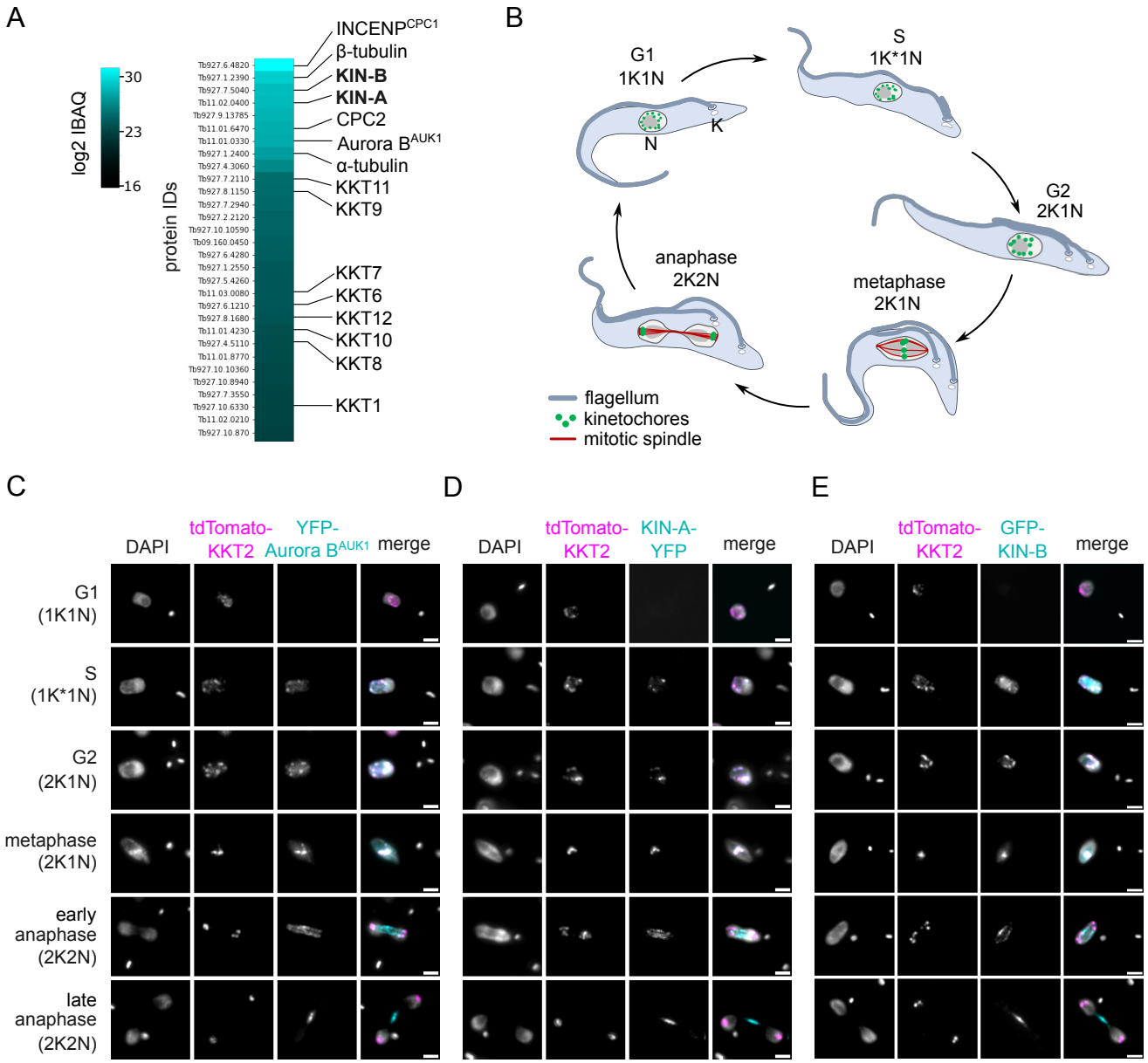
A
log2 IBAQ
30
23
16
protein IDs
INCENP^CPC1
β-tubulin
KIN-B
KIN-A
CPC2
Aurora B^AUK1
α-tubulin
KKT11
KKT9
KKT7
KKT6
KKT12
KKT10
KKT8
KKT1
B
G1
1K1N
N
K
S
1K*1N
G2
2K1N
metaphase
2K1N
anaphase
2K2N
flagellum
kinetochores
mitotic spindle
C
DAPI
tdTomato-KKT2
YFP-Aurora B^AUK1
merge
G1 (1K1N)
S (1K*1N)
G2 (2K1N)
metaphase (2K1N)
early anaphase (2K2N)
late anaphase (2K2N)
D
DAPI
tdTomato-KKT2
KIN-A-YFP
merge
E
DAPI
tdTomato-KKT2
GFP-KIN-B
merge

Figure 2

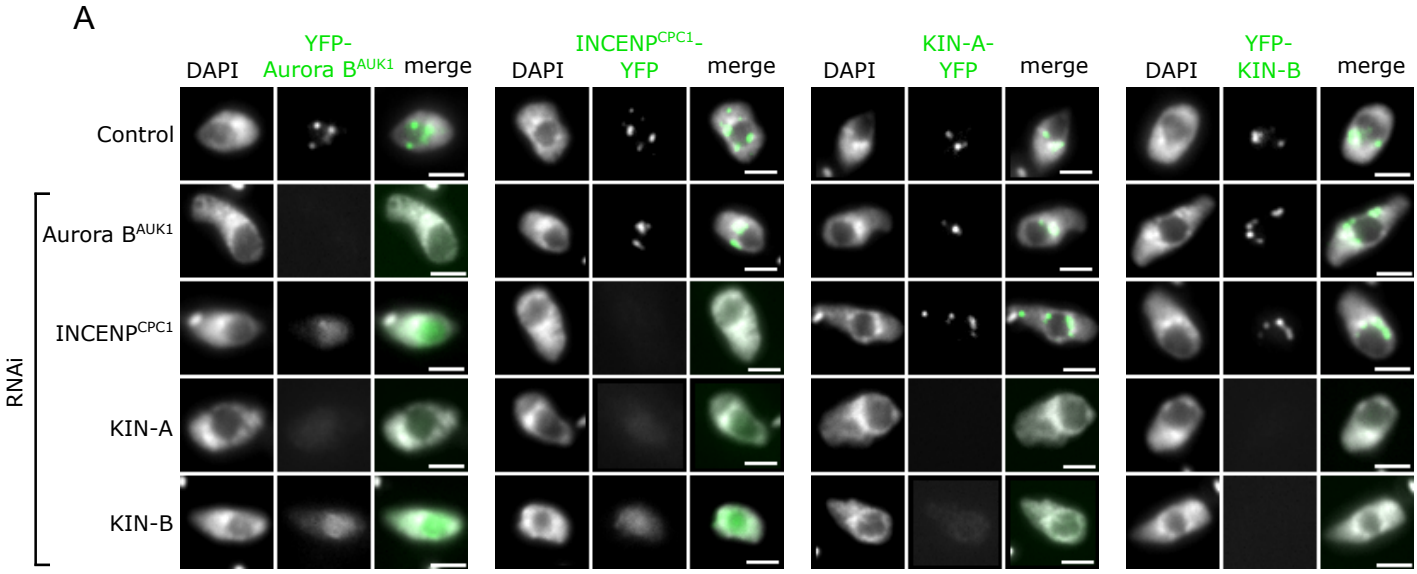
A
DAPI
YFP-Aurora B^AUK1
merge
INCENP^CPC1-YFP
KIN-A-YFP
YFP-KIN-B
Control
Aurora B^AUK1
INCENP^CPC1
KIN-A
KIN-B
RNAi

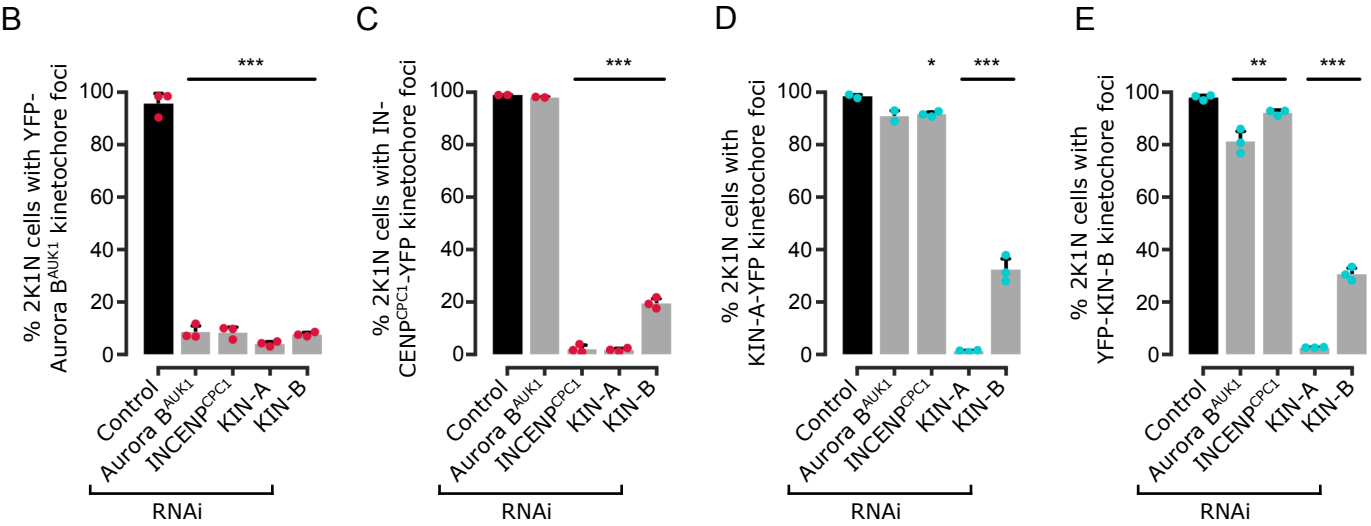
B
% 2K1N cells with YFP-Aurora B^AUK1 kinetochore foci
C
% 2K1N cells with IN-CENP^CPC1-YFP kinetochore foci
D
% 2K1N cells with KIN-A-YFP kinetochore foci
E
% 2K1N cells with YFP-KIN-B kinetochore foci
***
**
*
Control
Aurora B^AUK1
INCENP^CPC1
KIN-A
KIN-B
RNAi

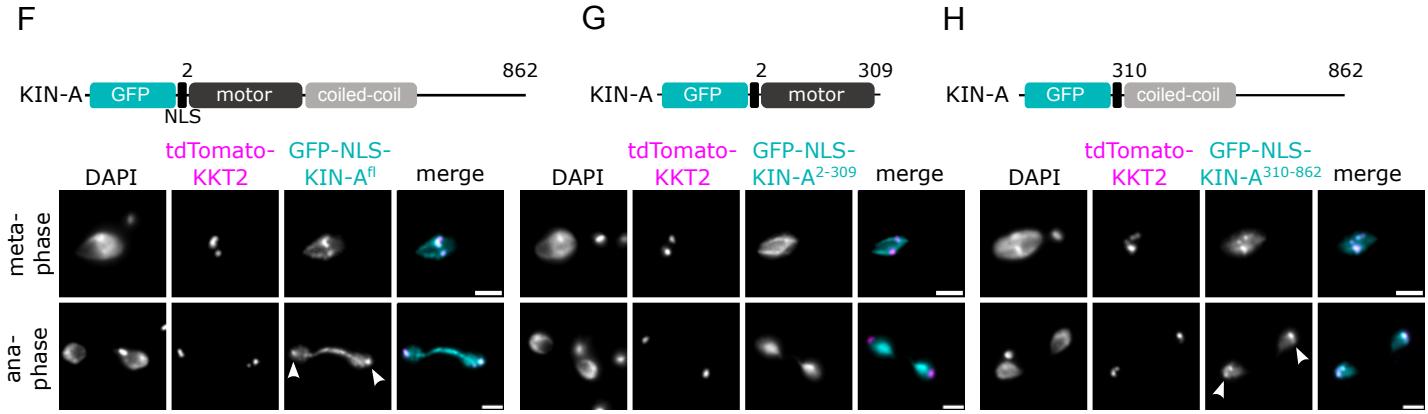
F
G
H
KIN-A-
GFP
NLS
motor
coiled-coil
2
862
309
310
DAPI
tdTomato-KKT2
GFP-NLS-KIN-A^fl
GFP-NLS-KIN-A^2-309
GFP-NLS-KIN-A^310-862
merge
meta-phase
ana-phase

Figure 3

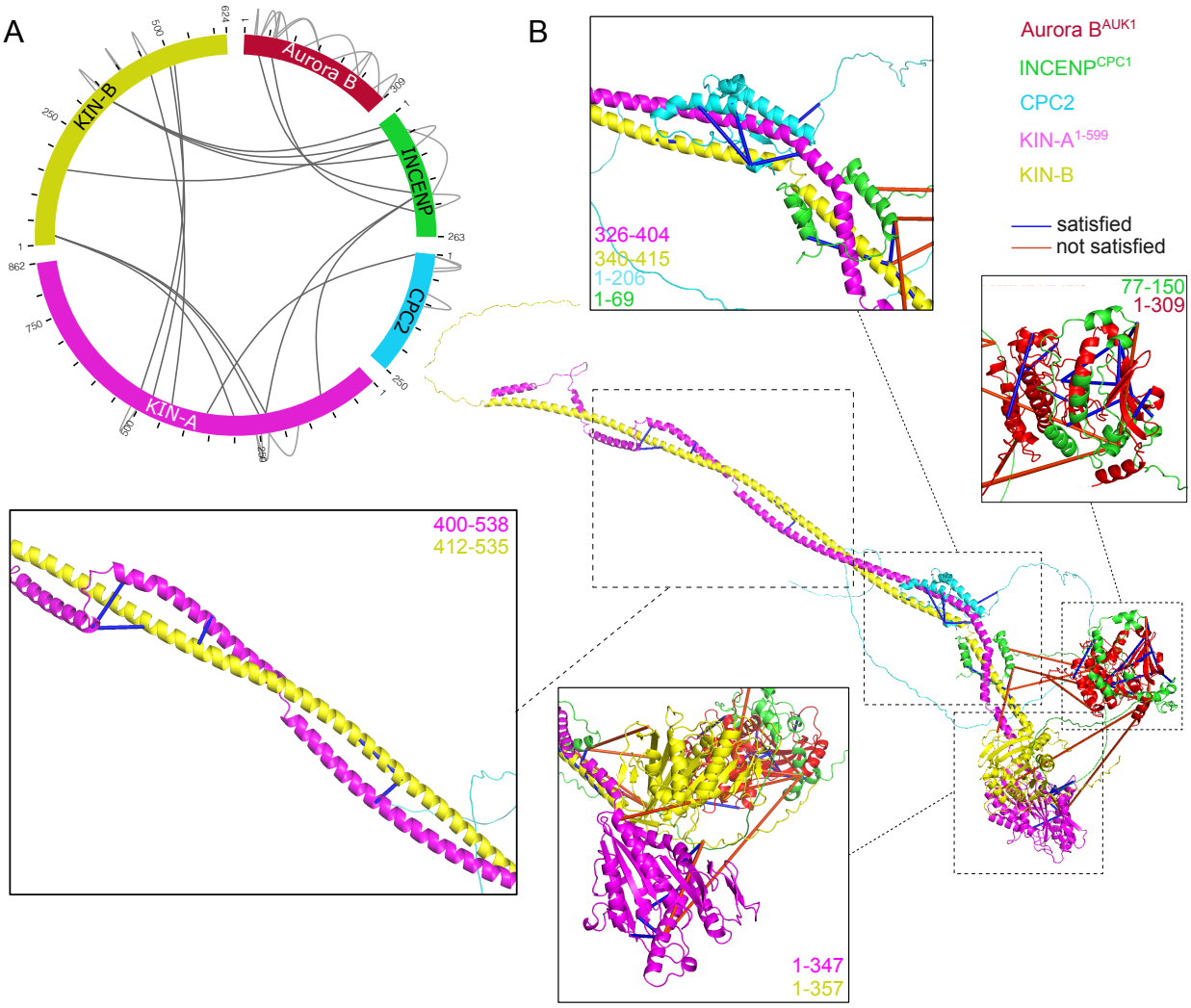
A
B
Aurora B
INCENP
CPC2
KIN-A
KIN-B
Aurora B^AUK1
INCENP^CPC1
CPC2
KIN-A^1-599
KIN-B
satisfied
not satisfied
326-404
340-415
1-206
1-69
77-150
1-309
400-538
412-535
1-347
1-357

Figure 4

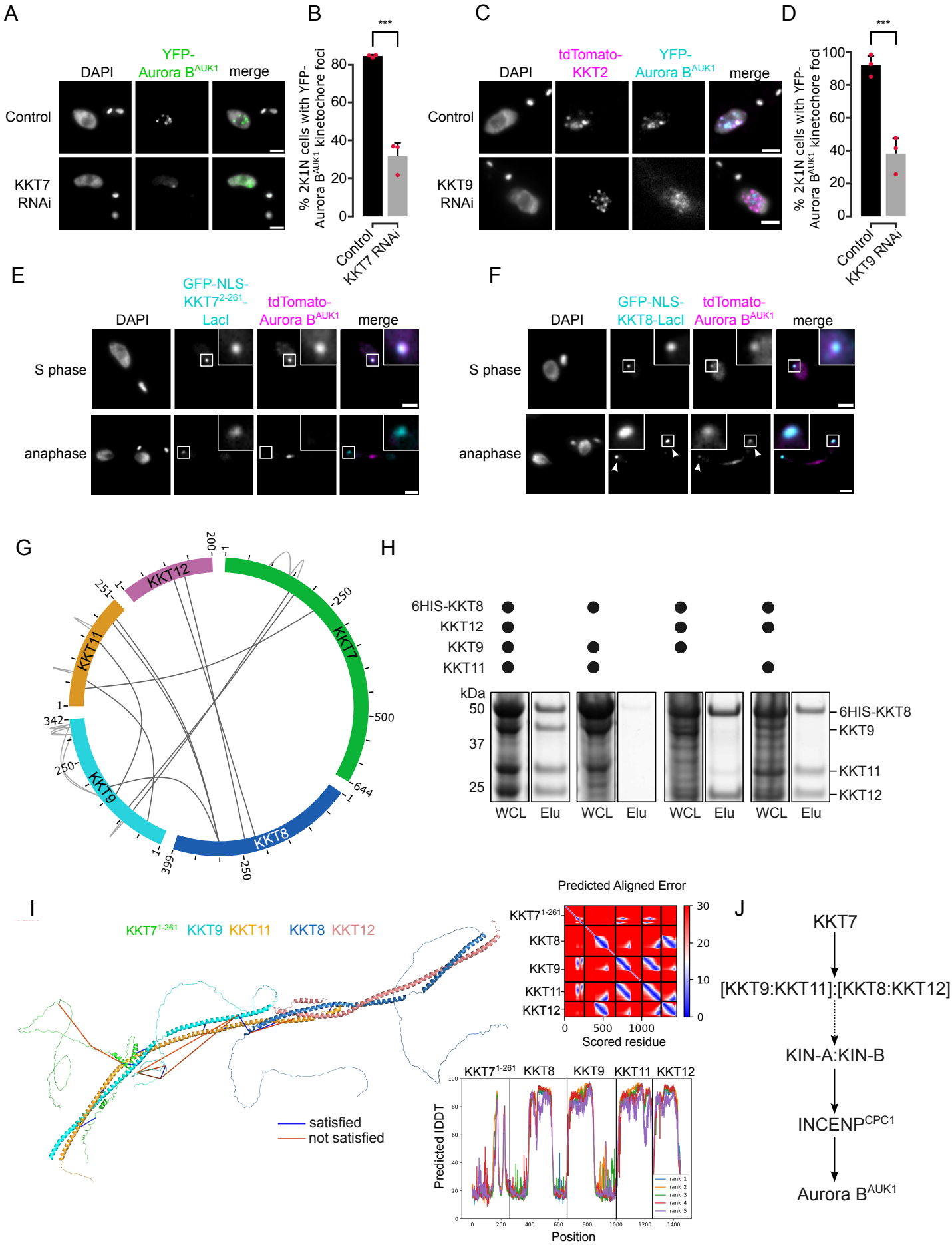
A
DAPI
YFP-Aurora B^AUK1
merge
Control
KKT7 RNAi
B
% 2K1N cells with YFP-Aurora B^AUK1 kinetochore foci
***
Control
KKT7 RNAi
C
DAPI
tdTomato-KKT2
YFP-Aurora B^AUK1
merge
Control
KKT9 RNAi
D
% 2K1N cells with YFP-Aurora B^AUK1 kinetochore foci
***
Control
KKT9 RNAi
E
DAPI
GFP-NLS-KKT7^2-261-LacI
tdTomato-Aurora B^AUK1
merge
S phase
anaphase
F
DAPI
GFP-NLS-KKT8-LacI
tdTomato-Aurora B^AUK1
merge
S phase
anaphase
G
KKT12
KKT7
KKT11
KKT9
KKT8
H
6HIS-KKT8
KKT12
KKT9
KKT11
kDa
50
37
25
WCL
Elu
6HIS-KKT8
KKT9
KKT11
KKT12
I
KKT7^1-261
KKT9
KKT11
KKT8
KKT12
satisfied
not satisfied
Predicted Aligned Error
Scored residue
Predicted lDDT
Position
J
KKT7
[KKT9:KKT11]:[KKT8:KKT12]
KIN-A:KIN-B
INCENP^CPC1
Aurora B^AUK1

Figure 5

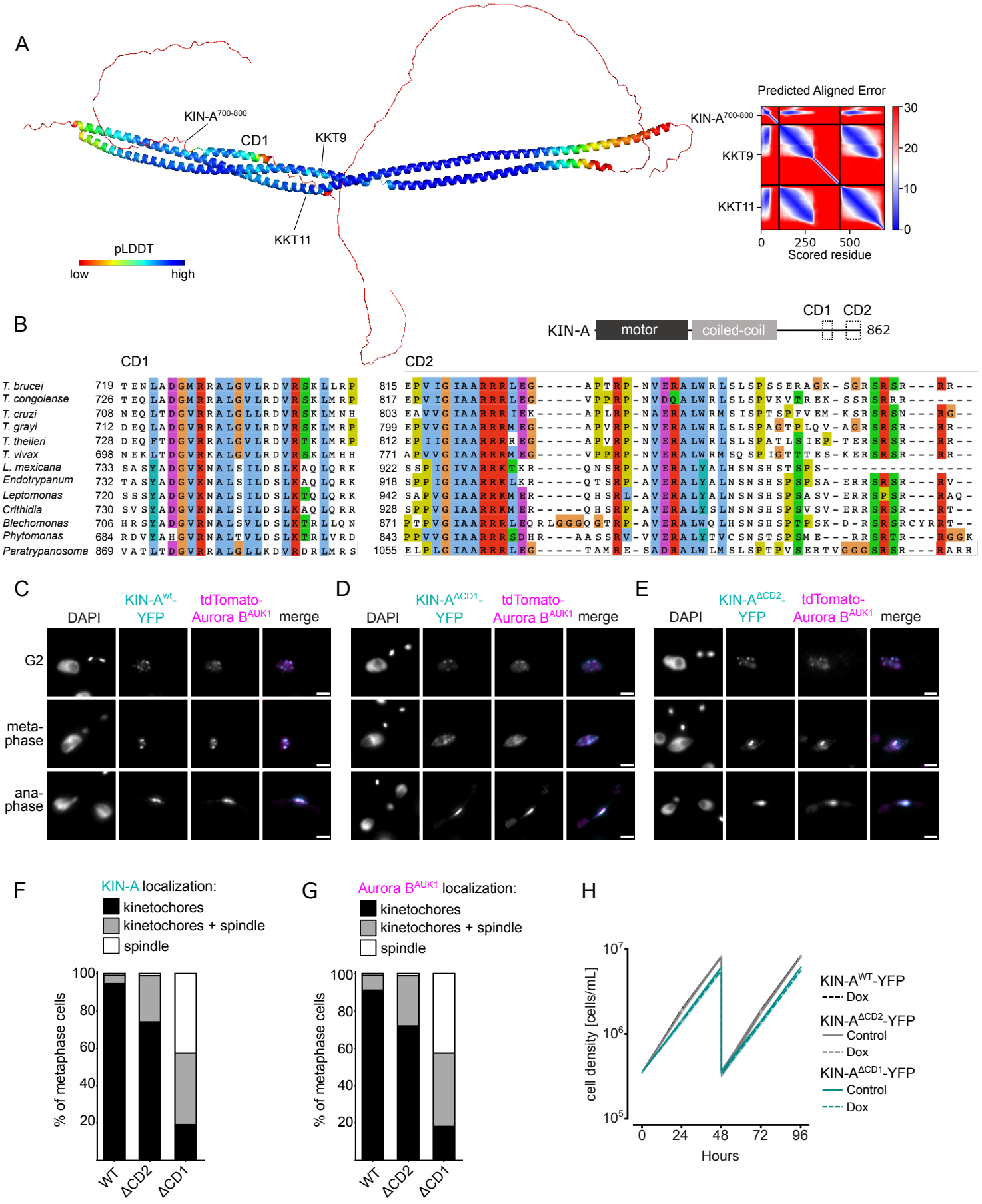
A
KIN-A700-800
CD1
KKT9
KKT11
pLDDT
low
high
Predicted Aligned Error
KIN-A700-800
KKT9
KKT11
0
250
500
Scored residue
30
20
10
0
B
CD1
CD2
KIN-A
motor
coiled-coil
862
T. brucei
T. congolense
T. cruzi
T. grayi
T. theileri
T. vivax
L. mexicana
Endotrypanum
Leptomonas
Crithidia
Blechomonas
Phytomonas
Paratrypanosoma
C
DAPI
KIN-Awt-YFP
tdTomato-Aurora BAUK1
merge
G2
meta-phase
ana-phase
D
KIN-AΔCD1-YFP
E
KIN-AΔCD2-YFP
F
KIN-A localization:
kinetochores
kinetochores + spindle
spindle
% of metaphase cells
WT
ΔCD2
ΔCD1
G
Aurora BAUK1 localization:
H
cell density [cells/mL]
Hours
KIN-AWT-YFP
Dox
KIN-AΔCD2-YFP
Control
KIN-AΔCD1-YFP

Figure 6

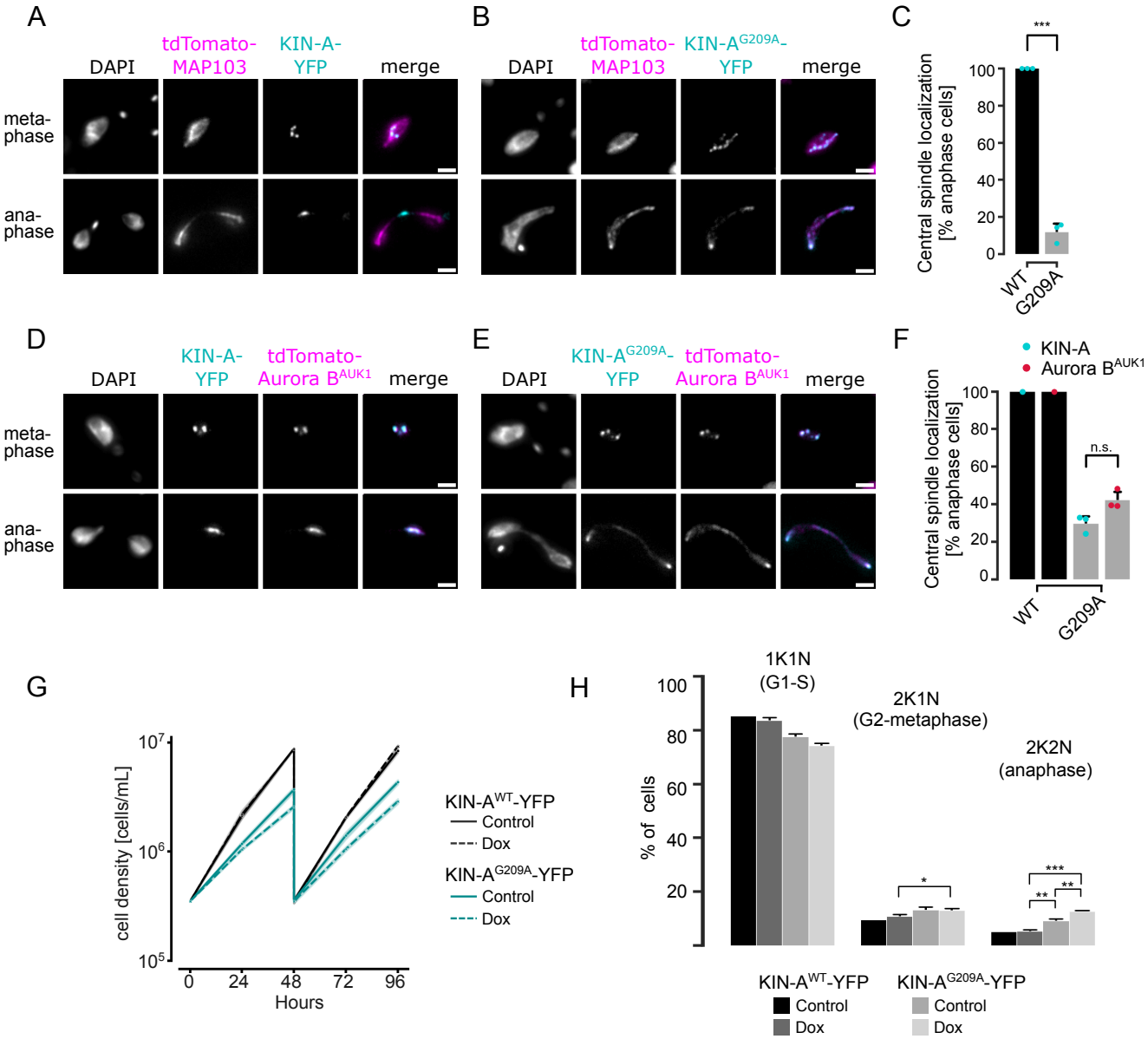
A
DAPI
tdTomato-MAP103
KIN-A-YFP
merge
meta-phase
ana-phase
B
DAPI
tdTomato-MAP103
KIN-A^{G209A}-YFP
merge
C
Central spindle localization [% anaphase cells]
***
WT
G209A
D
DAPI
KIN-A-YFP
tdTomato-Aurora B^{AUK1}
merge
E
DAPI
KIN-A^{G209A}-YFP
tdTomato-Aurora B^{AUK1}
merge
F
KIN-A
Aurora B^{AUK1}
n.s.
G
cell density [cells/mL]
Hours
KIN-A^{WT}-YFP
Control
Dox
KIN-A^{G209A}-YFP
Control
Dox
H
% of cells
1K1N (G1-S)
2K1N (G2-metaphase)
2K2N (anaphase)
KIN-A^{WT}-YFP
Control
Dox
KIN-A^{G209A}-YFP
Control
Dox

Figure S1

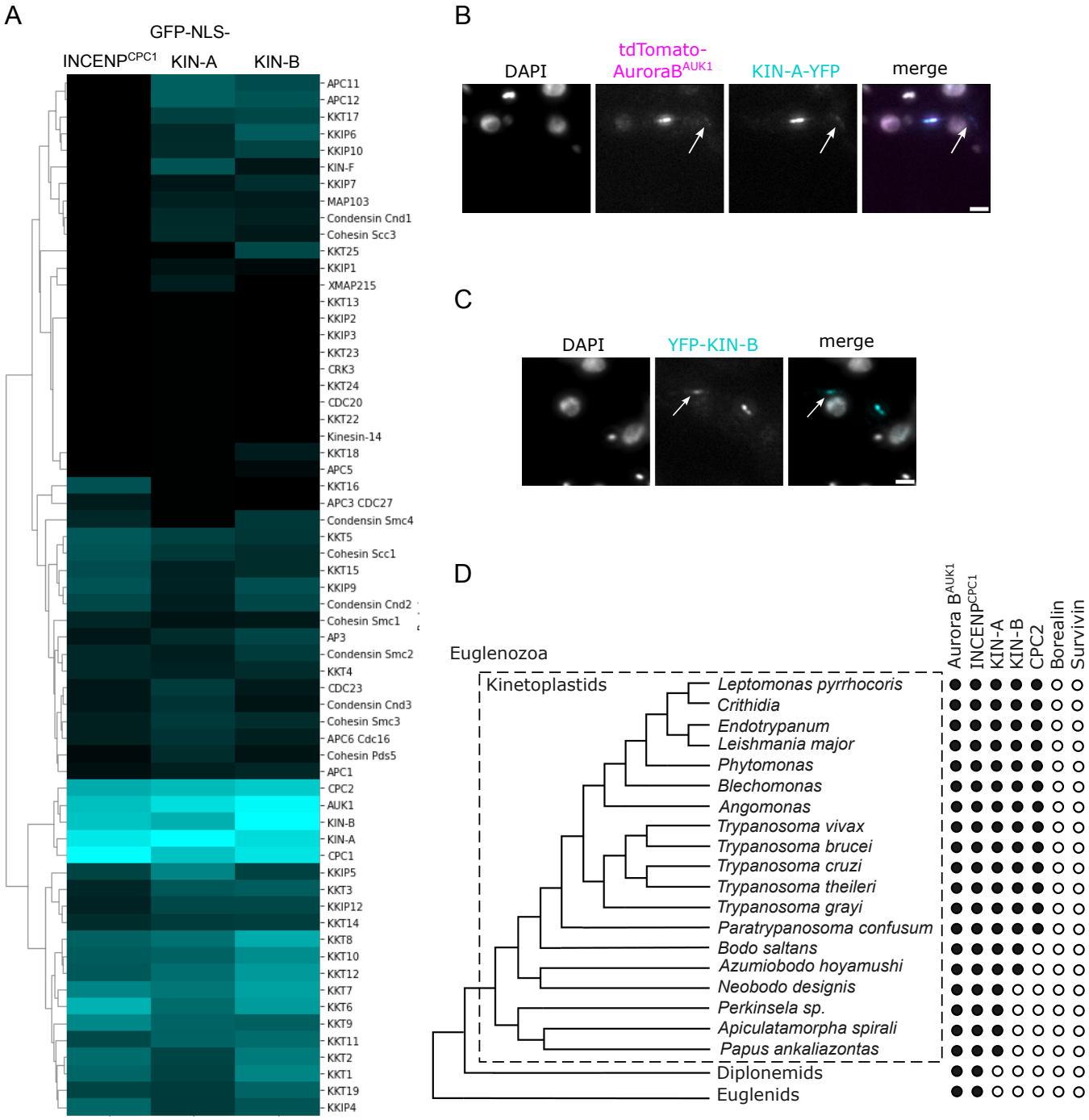
A
GFP-NLS-
INCENP^CPC1
KIN-A
KIN-B
APC11
APC12
KKT17
KKIP6
KKIP10
KIN-F
KKIP7
MAP103
Condensin Cnd1
Cohesin Scc3
KKT25
KKIP1
XMAP215
KKT13
KKIP2
KKIP3
KKT23
CRK3
KKT24
CDC20
KKT22
Kinesin-14
KKT18
APC5
KKT16
APC3 CDC27
Condensin Smc4
KKT5
Cohesin Scc1
KKT15
KKIP9
Condensin Cnd2
Cohesin Smc1
AP3
Condensin Smc2
KKT4
CDC23
Condensin Cnd3
Cohesin Smc3
APC6 Cdc16
Cohesin Pds5
APC1
CPC2
AUK1
KIN-B
KIN-A
CPC1
KKIP5
KKT3
KKIP12
KKT14
KKT8
KKT10
KKT12
KKT7
KKT6
KKT9
KKT11
KKT2
KKT1
KKT19
KKIP4
B
DAPI
tdTomato-AuroraB^AUK1
KIN-A-YFP
merge
C
DAPI
YFP-KIN-B
merge
D
Euglenozoa
Kinetoplastids
Leptomonas pyrrhocoris
Crithidia
Endotrypanum
Leishmania major
Phytomonas
Blechomonas
Angomonas
Trypanosoma vivax
Trypanosoma brucei
Trypanosoma cruzi
Trypanosoma theileri
Trypanosoma grayi
Paratrypanosoma confusum
Bodo saltans
Azumiobodo hoyamushi
Neobodo designis
Perkinsela sp.
Apiculatamorpha spirali
Papus ankaliazontas
Diplonemids
Euglenids
Aurora B^AUK1
INCENP^CPC1
KIN-A
KIN-B
CPC2
Borealin
Survivin

Figure S2

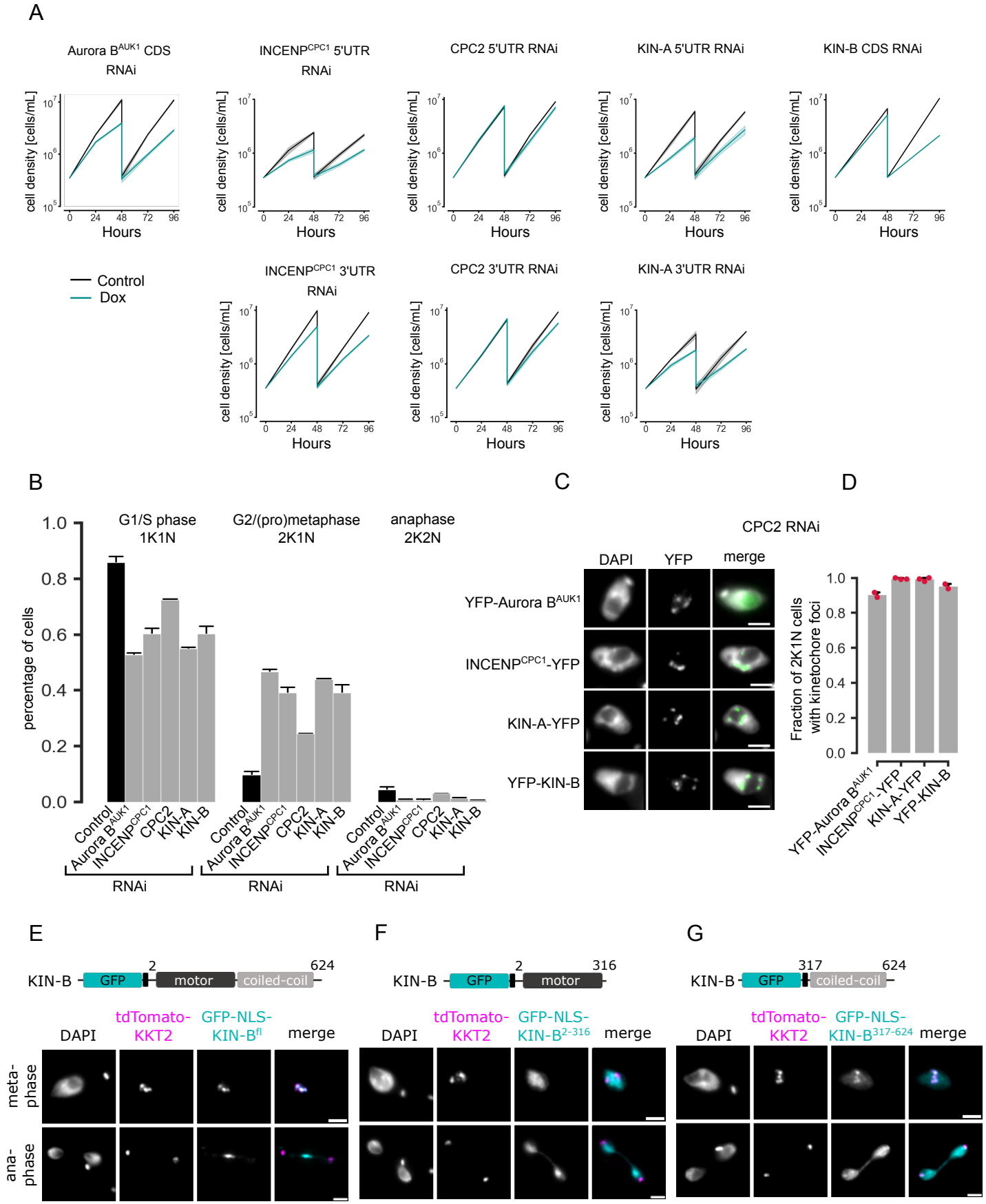
A
Aurora B^AUK1 CDS RNAi
INCENP^CPC1 5'UTR RNAi
CPC2 5'UTR RNAi
KIN-A 5'UTR RNAi
KIN-B CDS RNAi
INCENP^CPC1 3'UTR RNAi
CPC2 3'UTR RNAi
KIN-A 3'UTR RNAi
cell density [cells/mL]
Hours
Control
Dox
B
G1/S phase 1K1N
G2/(pro)metaphase 2K1N
anaphase 2K2N
percentage of cells
Control
Aurora B^AUK1
INCENP^CPC1
CPC2
KIN-A
KIN-B
RNAi
C
CPC2 RNAi
DAPI
YFP
merge
YFP-Aurora B^AUK1
INCENP^CPC1-YFP
KIN-A-YFP
YFP-KIN-B
D
Fraction of 2K1N cells with kinetochore foci
E
KIN-B
GFP
motor
coiled-coil
2
624
tdTomato-KKT2
GFP-NLS-KIN-B^fl
meta-phase
ana-phase
F
316
GFP-NLS-KIN-B^2-316
G
317
GFP-NLS-KIN-B^317-624

Figure S3

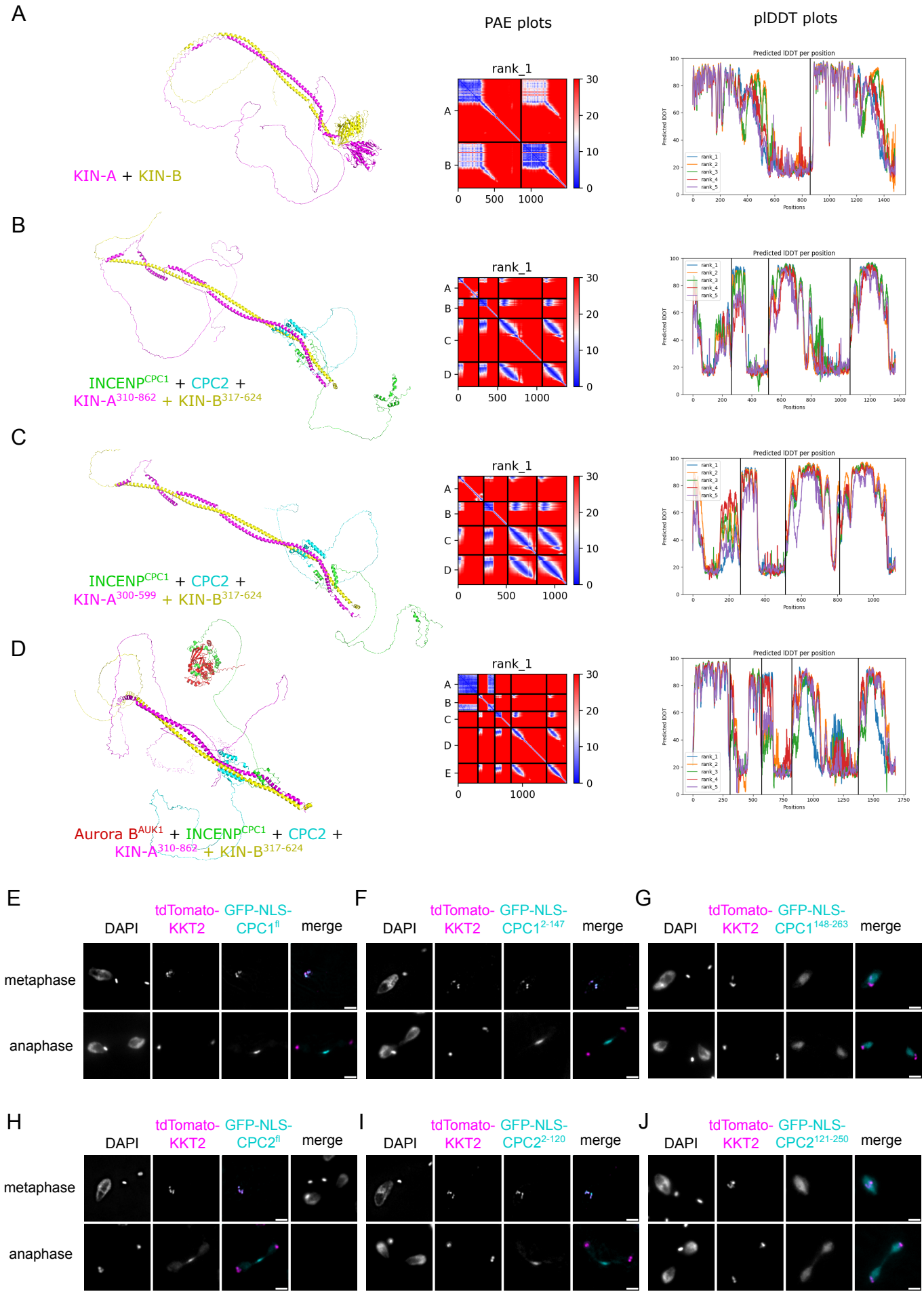
A
PAE plots
pIDDT plots
KIN-A + KIN-B
rank_1
Predicted lDDT per position
B
INCENP^CPC1 + CPC2 +
KIN-A^310-862 + KIN-B^317-624
C
INCENP^CPC1 + CPC2 +
KIN-A^300-599 + KIN-B^317-624
D
Aurora B^AUK1 + INCENP^CPC1 + CPC2 +
KIN-A^310-862 + KIN-B^317-624
E
DAPI
tdTomato-KKT2
GFP-NLS-CPC1^fl
merge
metaphase
anaphase
F
GFP-NLS-CPC1^2-147
G
GFP-NLS-CPC1^148-263
H
GFP-NLS-CPC2^fl
I
GFP-NLS-CPC2^2-120
J
GFP-NLS-CPC2^121-250

Figure S4

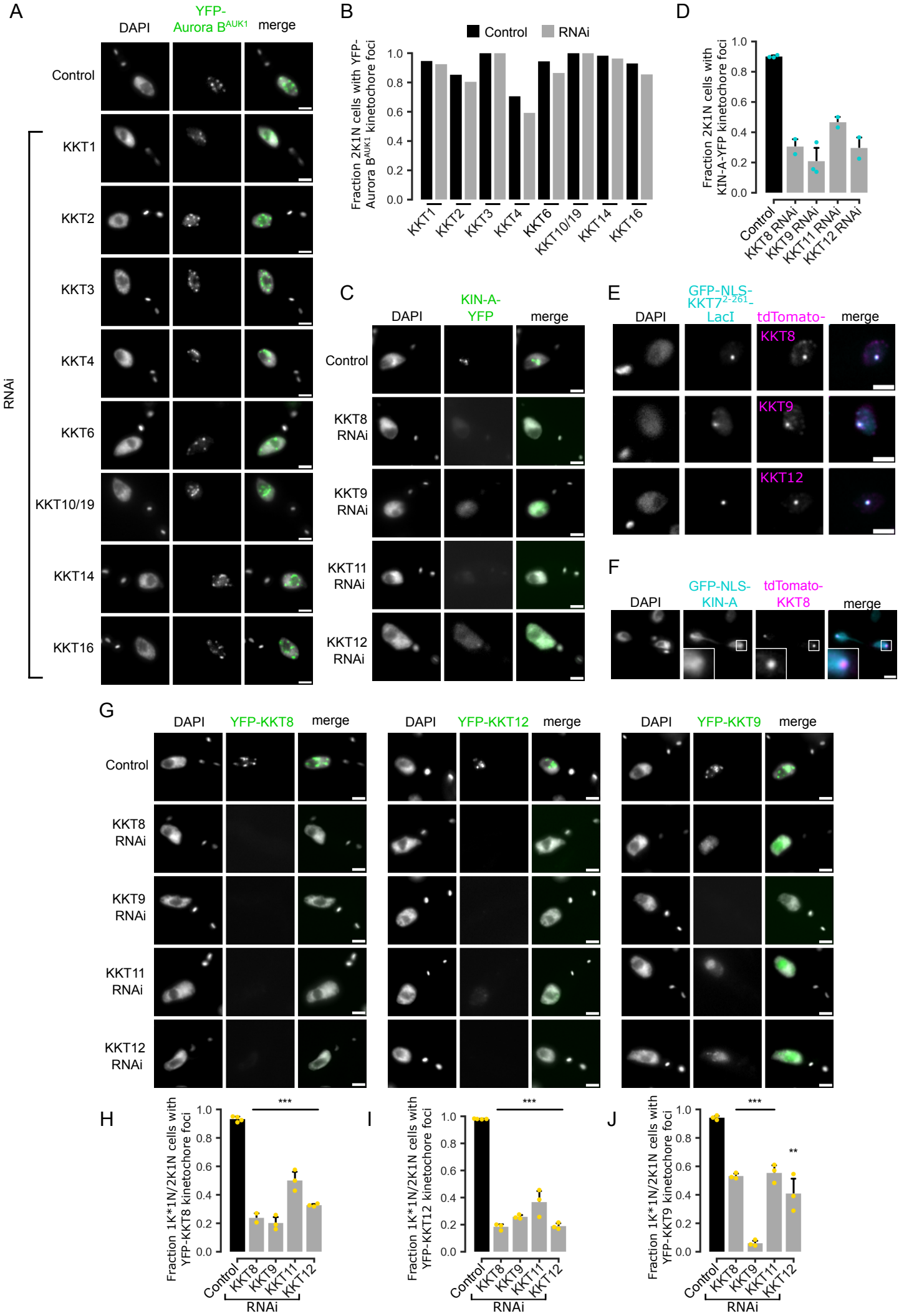
A
DAPI
YFP-Aurora B^AUK1
merge
Control
KKT1
KKT2
KKT3
KKT4
KKT6
KKT10/19
KKT14
KKT16
RNAi
B
Control
RNAi
Fraction 2K1N cells with YFP-Aurora B^AUK1 kinetochore foci
1.0
0.8
0.6
0.4
0.2
0.0
KKT1
KKT2
KKT3
KKT4
KKT6
KKT10/19
KKT14
KKT16
D
Fraction 2K1N cells with KIN-A-YFP kinetochore foci
Control
KKT8 RNAi
KKT9 RNAi
KKT11 RNAi
KKT12 RNAi
C
DAPI
KIN-A-YFP
merge
Control
KKT8 RNAi
KKT9 RNAi
KKT11 RNAi
KKT12 RNAi
E
DAPI
GFP-NLS-KKT7^2-261-LacI
tdTomato-KKT8
merge
KKT8
KKT9
KKT12
F
DAPI
GFP-NLS-KIN-A
tdTomato-KKT8
merge
G
DAPI
YFP-KKT8
merge
DAPI
YFP-KKT12
merge
DAPI
YFP-KKT9
merge
Control
KKT8 RNAi
KKT9 RNAi
KKT11 RNAi
KKT12 RNAi
H
Fraction 1K*1N/2K1N cells with YFP-KKT8 kinetochore foci
***
Control
KKT8
KKT9
KKT11
KKT12
RNAi
I
Fraction 1K*1N/2K1N cells with YFP-KKT12 kinetochore foci
***
Control
KKT8
KKT9
KKT11
KKT12
RNAi
J
Fraction 1K*1N/2K1N cells with YFP-KKT9 kinetochore foci
***
**
Control
KKT8
KKT9
KKT11
KKT12
RNAi

Figure S5

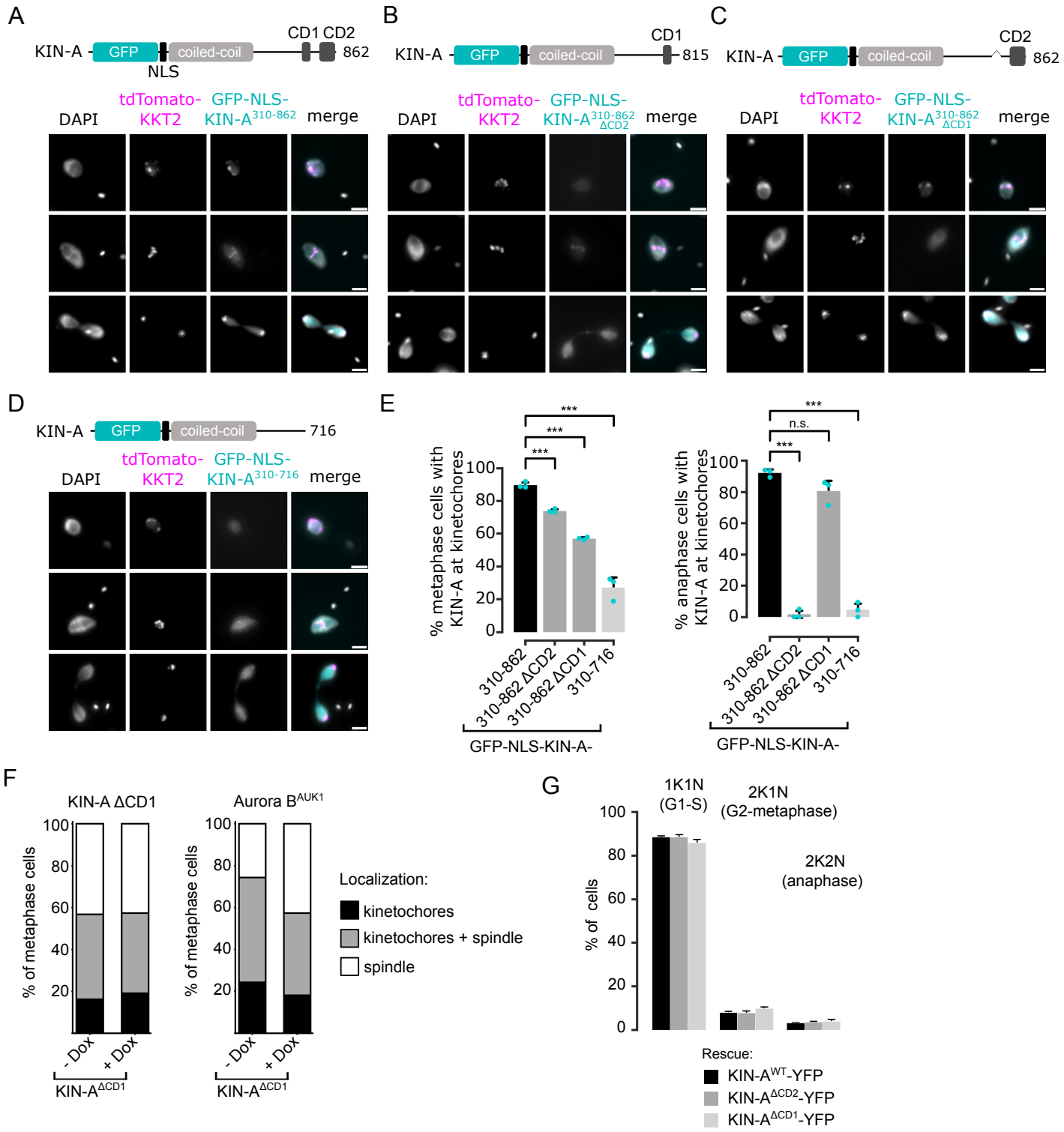
A
KIN-A
GFP
coiled-coil
NLS
CD1 CD2
862
DAPI
tdTomato-KKT2
GFP-NLS-KIN-A310-862
merge
B
KIN-A
GFP
coiled-coil
CD1
815
DAPI
tdTomato-KKT2
GFP-NLS-KIN-A310-862 ΔCD2
merge
C
KIN-A
GFP
coiled-coil
CD2
862
DAPI
tdTomato-KKT2
GFP-NLS-KIN-A310-862 ΔCD1
merge
D
KIN-A
GFP
coiled-coil
716
DAPI
tdTomato-KKT2
GFP-NLS-KIN-A310-716
merge
E
% metaphase cells with KIN-A at kinetochores
% anaphase cells with KIN-A at kinetochores
***
n.s.
310-862
310-862 ΔCD2
310-862 ΔCD1
310-716
GFP-NLS-KIN-A-
F
KIN-A ΔCD1
Aurora BAUK1
% of metaphase cells
- Dox
+ Dox
KIN-AΔCD1
Localization:
kinetochores
kinetochores + spindle
spindle
G
1K1N (G1-S)
2K1N (G2-metaphase)
2K2N (anaphase)
% of cells
Rescue:
KIN-AWT-YFP
KIN-AΔCD2-YFP
KIN-AΔCD1-YFP

Figure S6

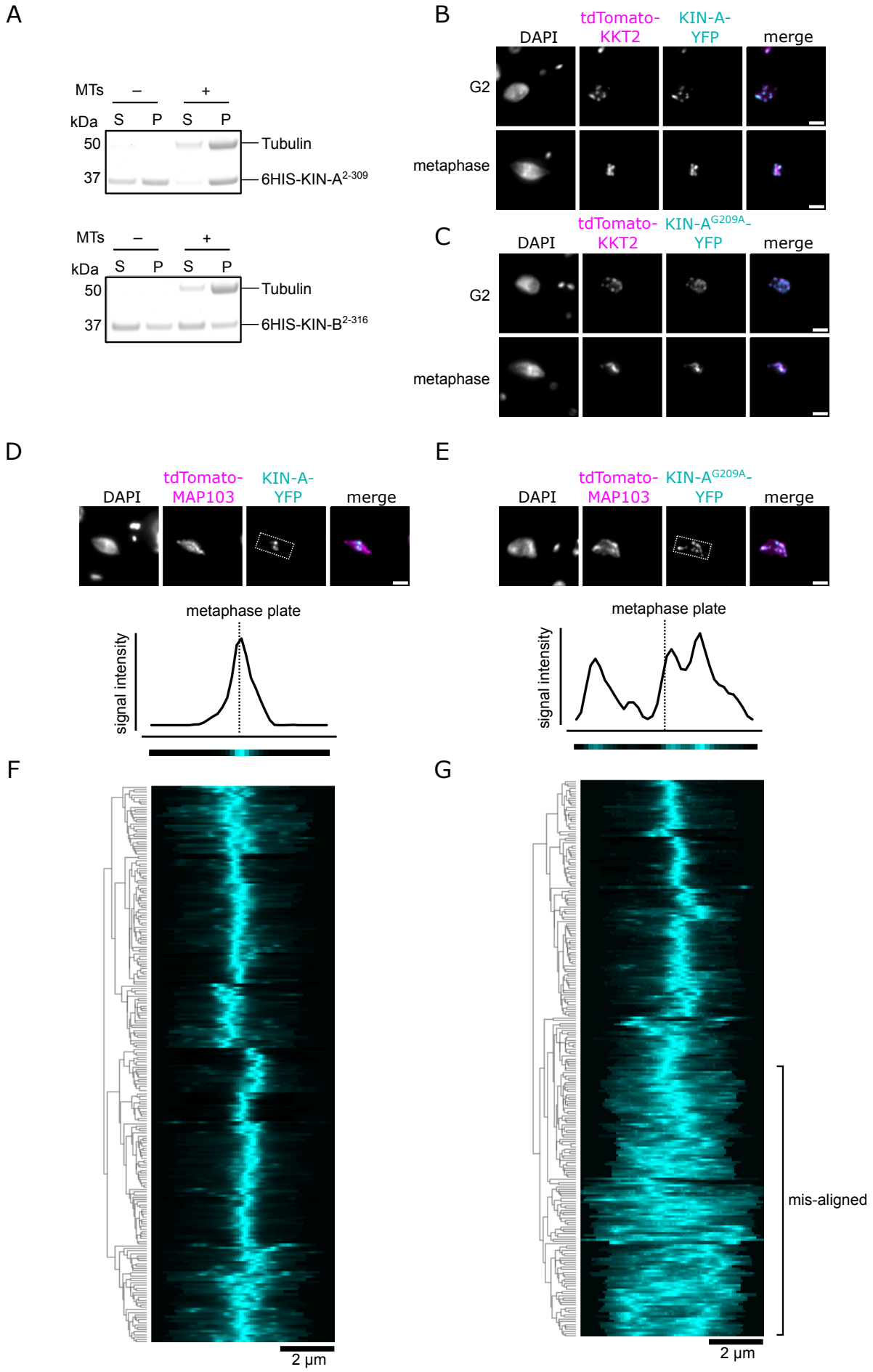
A
MTs
–
+
kDa
S
P
S
P
50
37
Tubulin
6HIS-KIN-A2-309
MTs
–
+
kDa
S
P
S
P
50
37
Tubulin
6HIS-KIN-B2-316
B
DAPI
tdTomato-KKT2
KIN-A-YFP
merge
G2
metaphase
C
DAPI
tdTomato-KKT2
KIN-AG209A-YFP
merge
G2
metaphase
D
DAPI
tdTomato-MAP103
KIN-A-YFP
merge
metaphase plate
signal intensity
E
DAPI
tdTomato-MAP103
KIN-AG209A-YFP
merge
metaphase plate
signal intensity
F
2 µm
G
mis-aligned
2 µm